ADAPTIVE PARAMETER SELECTION FOR DEEP BRAIN STIMULATION IN PARKINSON'S DISEASE

Mohammad Daneshzand

Under the Supervision of Dr. Miad Faezipour

DISSERTATION

SUBMITTED IN PARTIAL FULFILMENT OF THE REQUIREMENTS

FOR THE DEGREE OF DOCTOR OF PHILOSOPHY IN COMPUTER SCIENCE

AND ENGINEERING

THE SCHOOL OF ENGINEERING

UNIVERSITY OF BRIDGEPORT

CONNECTICUT

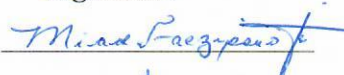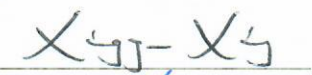May, 2019

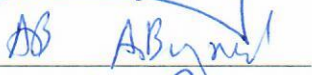# ADAPTIVE PARAMETER SELECTION FOR DEEP BRAIN STIMULATION IN PARKINSON'S DISEASE

Mohammad Daneshzand

Under the Supervision of Dr. Miad Faezipour

Approvals

Committee Members

Name	Signature	Date
Dr. Miad Faezipour	*Miad Faezipour*	3, 5, 2019
Dr. Buket D. Barkana (Co-Advisor)	*Buket Barkana*	3/5/19
Dr. Xingguo (Michael) Xiong	*XJJ-XJ*	03/05/19
Dr. Khaled Elleithy	*signature*	3/5/19
Dr. Abdelshakour Abuzneid	*AB ABuznd*	03-05-2019
Dr. Amalia Rusu	*Amalia Rusu*	3/5/19

Ph.D. Program Coordinator

Dr. Khaled M. Elleithy   *signature*   3/5/19

Chairman, Computer Science and Engineering Department

Dr. Ausif Mahmood   *Ausif Mahmood*   3-5-2019

Dean, School of Engineering

Dr. Tarek M. Sobh   *T. Sobh*   3/5/2019

ADAPTIVE PARAMETER SELECTION FOR DEEP BRAIN

STIMULATION IN PARKINSON'S DISEASE

ADAPTIVE PARAMETER SELECTION FOR DEEP BRAIN STIMULATION IN PARKINSON'S DISEASE

ABSTRACT

Each year, around 60,000 people are diagnosed with Parkinson's disease (PD) and the economic burden of PD is at least $14.4 billion a year in the United States. Pharmaceutical costs for a Parkinson's patient can be reduced from $12,000 to $6,000 per year with the addition of neuromodulation therapies such as Deep Brain Stimulation (DBS), transcranial Direct Current Stimulation (tDCS), Transcranial Magnetic Stimulation (TMS), etc. In neurodegenerative disorders such as PD, deep brain stimulation (DBS) is a desirable approach when the medication is less effective for treating the symptoms. DBS incorporates transferring electrical pulses to a specific tissue of the central nervous system and obtaining therapeutic results by modulating the neuronal activity of that region. The hyperkinetic symptoms of PD are associated with the ensembles of interacting oscillators that cause excess or abnormal synchronous behavior within the Basal Ganglia (BG) circuitry. Delayed feedback stimulation is a closed loop technique shown to suppress this synchronous oscillatory activity. Deep Brain Stimulation via delayed feedback is known to destabilize the complex intermittent synchronous states. Computational models of the BG network are often introduced to investigate the effect of delayed feedback high

frequency stimulation on partially synchronized dynamics. In this work, we developed several computational models of four interacting nuclei of the BG as well as considering the Thalamo-Cortical local effects on the oscillatory dynamics. These models are able to capture the emergence of 34 Hz beta band oscillations seen in the Local Field Potential (LFP) recordings of the PD state. Traditional High Frequency Stimulations (HFS) has shown deficiencies such as strengthening the synchronization in case of highly fluctuating neuronal activities, increasing the energy consumed as well as the incapability of activating all neurons in a large-scale network. To overcome these drawbacks, we investigated the effects of the stimulation waveform and interphase delays on the overall efficiency and efficacy of DBS. We also propose a new feedback control variable based on the filtered and linearly delayed LFP recordings. The proposed control variable is then used to modulate the frequency of the stimulation signal rather than its amplitude. In strongly coupled networks, oscillations reoccur as soon as the amplitude of the stimulus signal declines. Therefore, we show that maintaining a fixed amplitude and modulating the frequency might ameliorate the desynchronization process, increase the battery lifespan and activate substantial regions of the administered DBS electrode. The charge balanced stimulus pulse itself is embedded with a delay period between its charges to grant robust desynchronization with lower amplitude needed. The efficiency and efficacy of the proposed Frequency Adjustment Stimulation (FAS) protocol in a delayed feedback method might contribute to further investigation of DBS modulations aspired to address a wide range of abnormal oscillatory behaviors observed in neurological disorders.

Adaptive stimulation can open doors towards simultaneous stimulation with MRI recordings. We additionally propose a new pipeline to investigate the effect of Transcranial Magnetic Stimulation (TMS) on patient specific models. The pipeline allows us to generate a full head segmentation based on each individual MRI data. In the next step, the neurosurgeon can adaptively choose the proper location of stimulation and transmit accurate magnetic field with this pipeline.

To my loving mom and dad

And unborn two daughters and son

ACKNOWLEDGEMENTS

TABLE OF CONTENTS

LIST OF TABLES

LIST OF FIGURES

the network size.

ACRONYMS

BG	Basal Ganglia
CSF	Cerebrospinal Fluid
DBS	Deep Brain Stimulation
EMG	Electromyography
FAS	Frequency Adjustment Stimulation
GPe	Globus Pallidus externa
GPi	Globus Pallidus interna
GM	Grey Matter
HFS	High Frequency Stimulation
LFS	Low Frequency Stimulation
LFP	Local Field Potentials
PD	Parkinson's disease
SICN	Signed Inverse Condition Number
STN	Subthalamic Nucleus
Th	Thalamic
tDCS	transcranial Direct Current Stimulation
TMS	Transcranial Magnetic Stimulation
WM	White Matter

CHAPTER 1: INRTODUCTION

1.1   Research Problem and Scope

In most of the neurodegenerative disorders such as PD, neuronal activities show synchronized dynamics. DBS has shown to improve various symptoms associated with PD by desynchronizing these oscillations [4]. However, the underlying mechanism of DBS is not fully understood. Through a surgically implanted DBS device, high frequency pulses (> 130 Hz) are delivered to a target cell within the Basal Ganglia (BG) causing an improvement in motor symptoms [5]. It has been hypothesized that HFS acts as a reversible lesion which stops the dysfunctional regions within the BG [6]. Whatever might cause DBS to outperform the medications must be thoroughly investigated by various DBS therapy paradigms. Improving the symptoms while reducing the side effects cannot cope with the shorter temporal dynamics of PD in an open loop stimulation paradigm [7]. Therefore, there is a need for dynamic stimulation systems such as closed loop or delayed feedback DBS, which are capable of continually adopting the stimulus based on the aggregated neuronal firing patterns. It has been shown that closed loop DBS ameliorates akinesia and abnormal Cortico-BG discharges [8], improves therapeutic efficiency, increases battery lifespan, decreases tissue damage, and adjusts the oscillatory patterns [9-11]. Closed loop models usually use the Local Field Potential (LFP) of the targeted region as the control variable since it is highly correlated with changes in the motor system [12-14]. LFP is then

filtered and analyzed to be fed in a feedback algorithm. The decision of the feedback algorithm will set the next parameters for the DBS signal. For higher performance, the stimulation amplitude is reduced according to the amplitude of the filtered LFP signal [15]. Unlike open loop stimulation, these methods constantly monitor the synchronized state (usually through the recorded LFP signal) and the stimulation strength is adjusted according to the extent of synchrony.

1.2 Motivation behind the Research

Each year, around 60,000 people are diagnosed with Parkinson's disease (PD) and the economic burden of PD is at least $14.4 billion a year in the United States. Pharmaceutical costs for a Parkinson's patient can be reduced from $12,000 per year to $6,000 per year with the addition of neuromodulation therapies such as Deep Brain Stimulation (DBS). In neurodegenerative disorders such as PD, deep brain stimulation (DBS) is a desirable approach when the medication is less effective for treating the symptoms. DBS incorporates transferring electrical pulses to a specific tissue of the central nervous system and obtaining therapeutic results by modulating the neuronal activity of that region. Recently, many studies have shifted towards adjusting the amplitude of DBS signals to improve the therapeutic efficacy. There are several limitations with adjusting the stimulation strength (amplitude) such as low energy efficiency and low performance in neuronal activation of sub populations within the targeted area [12]. Also, modulating the strength of the stimulation signal and especially, reducing it in case of highly fluctuating neuronal activities, increases the synchronization rather than suppressing it [16]. Therefore,

we propose a new method focused on adjusting the frequency of the stimulation signal in which the amplitude of the stimulation is kept constant for better desynchronization effects.

There are other parameters that must be considered for optimum DBS effect such as selection of appropriate target cells that DBS is delivered to. Although targeting the STN or GPe neurons will reduce symptoms of PD such as dyskinesia, tremor and rigidity, the choice of DBS target is highly dependable on the patient's symptoms [11, 17]. The stimulation waveform has also shown to be directly related to the desynchronization process and the total amount of energy consumed [9]. Choosing an appropriate stimulation signal can increase the battery lifespan and reduce the demand for costly battery replacement surgeries [14]. We have used a biphasic pulse for stimulation with a delay period between the cathodic and anodic phases to improve the desynchronization process [9, 18]. The amount of necessary stimulation amplitude for desynchronization significantly drops by the mean of an interphase delay. Accordingly, the risk of charge deposit into the targeted area and tissue damage would be much lower [19].

It has been shown that Low Frequency Stimulation (LFS) in the range of (60-80 Hz) is more beneficial for patients with axial symptoms, while HFS is more applicable for tremor, rigidity and bradykinesia and neuronal oscillatory dynamics are mostly ameliorated by HFS due to the latching of the firing discharge time to the frequency of stimulation [20]. Moreover, the inhibition induced by HFS changes the mean firing rate of the STN neurons and alters the neurotransmitter release and antidromic activation of the BG cells. Since various symptoms of PD correlate with different ranges of stimulation frequencies, frequency adjustment might lead to more therapeutic effects.

Experimental studies investigated the effect of DBS on single cell level [21], but there are vast unknown information that can be extracted from neural network activity and its reaction to stimulation. There are several existing neural mass models aiming to understand ambiguities of DBS in the network level [3, 22]. The model in [23] focused on synaptic interaction between STN and GPe to be able to describe normal and PD conditions. Along all the computational models used in retrospective studies, we used a modified version of the BG network [3] to investigate the effect of DBS parameters. These biologically inspired models capture the characteristics of various nuclei, however, these models are computationally complex. Low dimensional models, on the other hand, reduce the computational costs while the lack of physiological implications make the LFP estimation and feedback control more challenging. To reduce the computational cost while considering neural interconnections and properties of each nuclei within the BG network, we propose new approaches to model BG neurons. Low cost computation of this model guarantees the simulation of large neuronal population. Additionally, the synaptic connections within all neurons must be incorporated into the models to examine the synchrony in the Cortico-BG network along with the LFP assessments.

1.3   Contributions of the Proposed Research

The contributions of this research are summarized as follows:

1.   **Hypebolic Model:** We propose a low cost computational model of spiking neurons. This model can help realize the neuronal interconnection issues which demonstrate various neuronal behavior observed in vivo through simple parameter modification. The behaviors include tonic and phasic spiking, tonic and phasic bursting, class 1 and class 2 excitability,

rebound spike, rebound burst, sub threshold oscillation, accommodated spiking along with inhibition neuron responses. We investigate the neuronal spiking patterns in Parkinson's disease through our proposed model. Abnormal pattern of Subthalamic Nucleus (STN) in PD is studied through variations in the shape and frequency of firing patterns. Our proposed model introduces mathematical equations where these patterns can be derived and clearly differentiated from one another. The irregular and arrhythmic behavior of STN firing pattern under normal conditions can easily be transformed to those caused by PD through simple parameter modifications in the proposed model. This model can explicitly show the change of neuronal activity patterns in PD, which may eventually lead to effective treatment with deep brain stimulation devices.

2. **Novel DBS Waveforms:** We used the new hyperbolic neuronal spiking formulation along with Hodgkin-Huxley equations [1] in a mass model of BG to investigate the effect of the stimulation waveform [9]. Additionally, we tested the effect of stimulation interphase delay on the suppression of pathological oscillations seen in the model of PD. Optimized waveforms could prolong battery life, reduce the frequency of recharge intervals and reduce the cost and risk of battery replacement surgeries. The combinational DBS waveform with a delay between the anodic and cathodic phases allows for energy consumption reduction in the BG network along with the reduction of the number of times that DBS waveform fails to elicit an action potential. Experimental results show that this new DBS waveform can activate the BG neurons with lower amplitude and shorter duration of delay compared to previously used DBS signals such as rectangular pulses. This new waveform modification also improves the synchrony of DBS pulses with firing of the BG

neurons; i.e. it was able to elicit an action potential on the applied neuron with almost every pulse of the DBS signal [9].

3.   **DBS Targets:** Additionally, we investigate the effect of an optimized waveform such as Gaussian DBS signals on different targets of BG containing STN, GPe and GPi neurons. As has been studied by many researchers, Gaussian waveforms can elicit APs in the BG region with lower amount of energy consumption, which reduces the need of battery replacement surgeries. With our model and simulations, we observed that the neuronal response of PD patients with gait dyskinesia are better treated by GPi-DBS rather than STN-DBS due to the fact that higher Action Potentials (APs) caused by STN-DBS leads to dyskinetic side effects. Bradykinesia and akinesia symptoms of PD can be treated better with GPe-DBS, since it generates less APs. Both STN-DBS and GPi-DBS produced better results for the desynchronization of GPi neurons and therefore can be used to improve the axial and cardinal symptoms of PD patients. Additionally appropriate targets

4.   **Frequency Adjustment Stimulation (FAS):** To reduce the computational cost of BG models while considering neural interconnections and properties of each nuclei within the BG network, we propose a 3 dimensional model based on the Izhikevich formulation [2]. Low cost computation of this model guarantees the simulation of large neuronal population. Our model is able to generate the membrane voltages of the BG neurons, temporal firing patterns, and synchrony dynamics seen in experimental recordings[21]. Improving the symptoms while reducing the side effects cannot cope with the shorter temporal dynamics of PD in an open loop stimulation paradigm [7]. Therefore, there is a need for dynamic stimulation systems such as closed loop [24] or delayed feedback DBS,

which are capable of continually adopting the stimulus based on the aggregated neuronal firing patterns.

We propose a new frequency adaptation stimulus according to the variation of LFP in a closed loop model. Our protocol adjusts the frequency of stimulation according to the level of synchrony observed by the LFP signal [25]. For instance, HFS is only applied at the peaks of the LFP signal where the synchronization is relatively high and the stimulation frequency declines as the synchronization level reduces. Closed loop adjustment of the frequency of stimulation shows better desynchronization while being energy efficient [26]. In addition, frequency adaptation has more therapeutic effects since various symptoms of PD correlate with different range of stimulation frequencies [27, 28]. Furthermore, a new pipeline for TMS navigation is proposed to improve the quality of patient specific models while providing a tool for clinicians to better target and stimulate brain regions.

CHAPTER 2: LITERATURE REVIEW

2.1 DBS for Parkinson's disease

Neuromodulation is a fast growing field of study focusing on methods of interfering with neuronal activity. Electrical stimulation such as DBS influences a wide variety of mechanisms at neuronal and system level [29]. Parameter configuration of DBS differs from patient to patient and requires experimental and computation models for obtaining a decent efficiency [30]. DBS disrupts the oscillatory activity of cells within the basal ganglia [31, 32]. The previous hypotheses about the mechanism of DBS were based on the idea of regularizing pathological activity through entrainment and synaptic modifications [23, 33], while recent studies elucidated that DBS on STN causes complex changes in the firing rate of efferent structures [34].

High frequency DBS (more than 100 Hz) has more therapeutic effect than low frequency stimulations, and this effect would increase if pulses are given at a specific phase [35]. Efficient stimulus waveforms must be able to elicit action potentials that subsequently lead to release of neurotransmitter while minimizing the side effects such as tissue damage, charge injection decrease and increase in energy consumption [36, 37]. Recent stimulators have charge balanced waveforms with short duration, high amplitude followed by long duration, low amplitude pulses. One of the optimal DBS waveforms which decreases energy consumption is an exponentially growing pulse by [38].[14] found a Gaussian waveform using the genetic algorithm to be the most optimal waveform. Most of implanted stimulators generate a high frequency pulse train [39]. In order to have

a charge balanced efficient stimulus pulse for PD, these pulses should have an amplitude around 3V and a frequency of 130 Hz [40]. A prolonged delay between the two parts of the charge balanced stimulation pulse improves activation of the resting neurons while entrainment of the bursting neurons [15].

There are several open loop stimulation protocols such as HFS and LFS where the stimulation parameters are fixed. More recent approaches tend to adjust the stimulation parameters in a closed loop paradigm. In this manner the recordings of BG is used as a control variable to adjust the stimulation parameters. Computational or mathematical models of BG neurons are widely used to test these various stimulation protocols [3, 9, 16, 18, 22, 41, 42].

2.2   Computational Neuroscience

Computational neuroscience is the science of studying the brain function with computer science modeling, and looking at all of the activity of the human brain through the lens of computer science. Since any brain disorder involves a group of neurons, a computationally efficient neuron model can help understand the behavior of a large group of coupled neurons, while providing low computational complexity is of high significance [43]. Computational models of neuronal activity can be divided in two categories:

- Biologically inspired models
- Low computational cost models

The biologically inspired models tend to define the neuronal activity based on the membrane potentials of a neuron. Although these models try to incorporate the

electrophysiological phenomena of a neuron, their large amount of differential equations make them difficult to be applied in neuronal population models [1]. On the other hand, the low computational cost models are defined to decrease the amount of computation, while generating similar firing patterns to biologically inspired or experimental recordings [2]. Here we explain 2 of the most used biologically inspired and low computational cost models for a single neuron.

2.3   Hodgkin-Huxley Neuronal Equations

Hodgkin and Huxley [1] proposed a simple biologically inspired model of a single neuron which eventually granted a Nobel Prize for the authors. Their model escribes how action potentials in neurons are initiated and propagated. They defined a set of nonlinear differential equations that approximates the electrical characteristics of excitable cells such as neurons. They showed that the chemical characteristics of a neuron can be represented by an electric circuit shown in Figure 2.1. In this Figure, each ion entering the neuron is faced by a resistor depicting the membrane resistance.
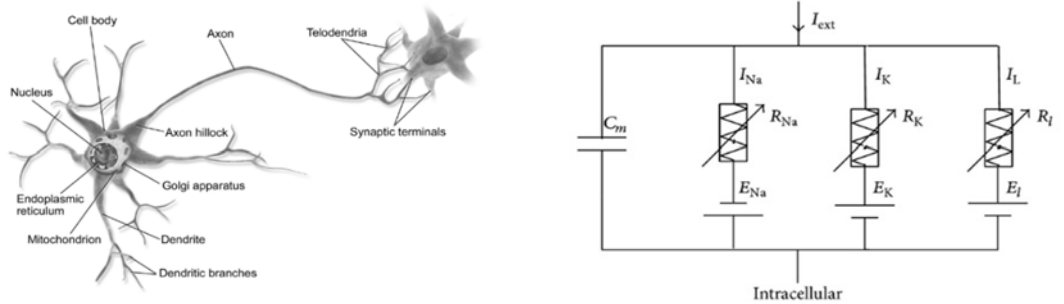
Figure 2.1. The Hodgkin Huxley neuronal circuitry [1]

The governing equations for defining the membrane voltage are defined as follows:

$$c_m \frac{dV}{dt} = I_{ext} - I_{Na} - I_K - I_l \qquad (2.1)$$

$$I_{Na} = g_{Na} m_\infty^3(V) h (V - V_{Na}) \qquad (2.2)$$

$$I_K = g_K n^4 (V - V_K) \qquad (2.3)$$

$$I_L = g_L (V - V_L) \qquad (2.4)$$

where the membrane voltage V of a neuron is defined by various intra and extra cellular currents and the membrane capacitance C_m. The I_L, I_{Na}, I_K and I_{ext} parameters represent leak, sodium, potassium and external currents, respectively. The governing equations for these currents are shown in Equations 2.2-2.4. The activation and inactivation parameters in Equations 2.2-2.4 are calculated according to the Equations below, assuming p can be any of the [n, m, h] parameters.

$$\varphi_p \frac{dp}{dt} = (p_\infty(V) - p)/\tau_p(V) \qquad (2.5)$$

$$p_\infty(V) = 1/(1 + e^{\left(-\frac{V-\theta_p}{\sigma_p}\right)}) \qquad (2.5a)$$

$$\tau_p(V) = \tau_p^0 + \tau_p^1/(1 + e^{\left(\frac{V-\theta_p^\tau}{\sigma_p^\tau}\right)}) \qquad (2.5b)$$

The parameters n, m, and h are dimensionless quantities between 0 and 1 that are associated with potassium channel activation, sodium channel activation, and sodium channel inactivation, respectively. Although the Hodgkin-Huxley equations capture the main ionic currents of a cell, they show a very high computational cost. The number of floating points for 1 mS of simulation of the Hodgkin-Huxley model is shown to be 1,200

11

[2]. Also, in order to model the BG neurons such as STN we need to extend the Hodgkin Huxley formulation as below, which drastically increases the computational cost.

$$C_m \frac{dV}{dt} = -I_L - I_{Na} - I_{Ca} - I_K - I_T - I_{ahp} - I_{Syn} - I_{app} \qquad (2.6)$$

where the membrane voltage V of each neuron is defined by various intra and extra cellular currents and the membrane capacitance C_m. The I_L, I_{Na}, I_{Ca}, I_K, I_T, I_{ahp}, I_{Syn} and I_{app} parameters represent leak, sodium, high threshold calcium, potassium, low threshold calcium, after hyperpolarization potassium, synaptic and external currents, respectively. The governing equations for these currents are shown below:

$$I_{Ca} = g_{Ca} s_\infty^2(V)(V - V_{Ca}) \qquad (2.7)$$

$$I_{T/STN} = g_T a_\infty^3(V) b_\infty^2(r)(V - V_{Ca}) \qquad (2.8)$$

$$I_{T/GPe} = g_T a_\infty^3(V) r(V - V_{Ca}) \qquad (2.9)$$

$$I_{ahp} = g_{ahp}(V - V_K)(Ca/Ca + K_I), \quad \epsilon \frac{dCa}{dt} = --I_{Ca} - I_K - K_{ca}Ca \qquad (2.10)$$

$$I_{Syn} = g_{Syn}(V - V_{Syn}) \sum_{i=1}^{N_{Syn}} s_i \qquad (2.11)$$

The numerical values for all parameters can be found in [18].

2.4 Izhikevich Model

A computationally efficient model of cortical neuron was proposed by Izhikevich in 2004 [2]. With simple polynomial differential equations, Izhikevich was able to

generate 20 different firing patterns seen in experimental recordings of human brain cells, as shown in Figure 2.2.
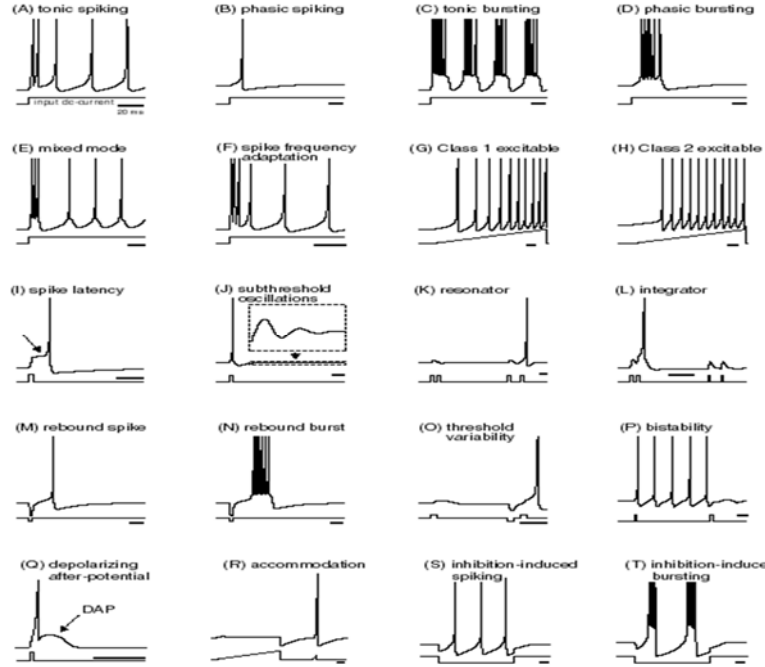
Figure 2.2 Various firing patters generated by Izhikevich Model [2]

The number of floating points for 1 mS of simulation with Izhikevich formulation was as low as 13 [2]. The governing equations of this model are as follows:

$$\frac{dV}{dt} = I_{ext} + 0.04\ V^2 + 5V + 140 - u \qquad (2.12)$$

$$\frac{du}{dt} = a(bV - u) \qquad (2.12a)$$

$$If\ V > 30\ mV \quad then \quad V = c \quad \& \quad u = u + d \quad (2.12b)$$

where a, b, c and d are set for the recovery time constant, resonance, potential reset value and outward minus inward currents activated during the spike and affecting the after-spike behavior, respectively (Figure 2.3).

13
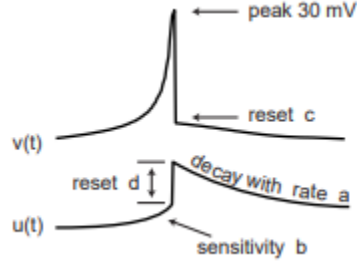
Figure 2.3 Parameters of Izhikevich model [23]

2.5 Computational models of BG

There has been numerous computational models of BG in the literature that try to explain and understand the underlying mechanism of DBS [3, 22, 23]. Most of these models have used the Hodgkin Huxley equations to generate the neuronal activities of STN, GPe, GPi and Thalamic neurons with their synaptic connections. The problem with these models arises when one attempts to generate a large population of these neurons for instance 1,000 neurons in each nucleus. Therefore, new approaches have moved toward more robust and fast models such as Izhikevich formulation. The schematic of BG area and its corresponding population model is shown in Figure 2.4 [3]. Each neuron type in this Figure follows an extended version of Hodgkin-Huxley model and the synaptic connections between these nuclei are defined as below:

$$I_{ion} = g_{ion}m_\infty^M h_\infty^N(V - E_{ion}) \qquad (2.13)$$

where g_{ion} is the conductance variable of each ion to or from the cell and m_∞^M and h_∞^N are activation and inactivation functions varying slightly for each involving ion in the cell [1]. V is the membrane potential and E_{ion} is the equilibrium potential of the ion.
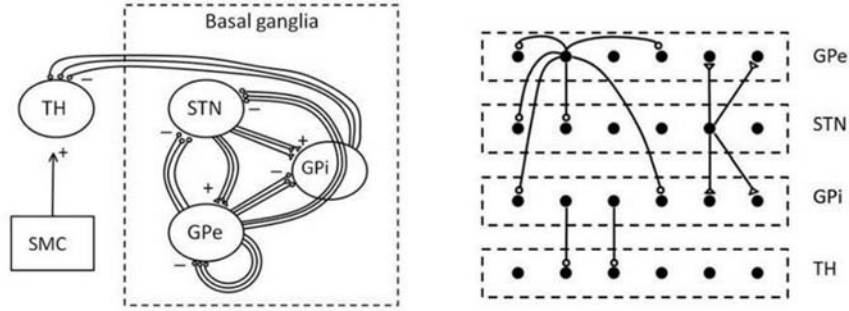
Figure 2.4 BG network model [3]

More recent models tend to understand the effects of DBS on the axonal and afferent network. For these goals, volumetric models have been developed with the capability to show the effect of DBS in a wider range [44]. These models can be used with the Magnetic Resonance Images (MRI) of each patient to detect the optimal DBS lead location and provide better insight on how DBS is affecting the targeted region.

2.6   DBS Target Selection

The optimal target to implement DBS within the basal ganglia depends on intraoperative targeting, electrophysiology, and macro stimulation, while preoperative targeting could be influenced by the standard stereotactic coordinates [45]. STN and GPi are the most commonly known target sites in the brain for both DBS and lesioning. Targeting STN and GPi neurons for DBS enhances the cardinal features of PD, such as rigidity, bradykinesia and tremor [46]. DBS targeted at STN (STN-DBS) could increase the risk of dyskinetic more than GPi-DBS [47]. A recent analysis of patients' outcomes shows that there is a comparable improvement for patients under STN-DBS and GPi-DBS in motor function and in the performance of daily activities after the surgery [48]. Recent studies show that targeting GPe for DBS has improved the symptoms of PD patients in terms of bradykinesia, akinesia, and rigidity in comparison to GPi-DBS [49].

All STN-DBS, GPi-DBS or GPe-DBS use the rectangular stimulus waveforms. Although rectangular waveforms have proven themselves efficient for deployment in clinical utilities, non-rectangular waveforms have offered certain advantages for neuromodulation devices [37]. The principle of selecting the stimulus waveform is to enable the generation of an appropriate neural response with less risk of stimulation induced tissue damage and less energy consumption [50]. The waveforms used in clinical DBS surgeries are mostly symmetric and charge-balanced rectangular waveforms with a high-amplitude, short-duration cathodic phase followed by a low amplitude, long-duration anodic phase. Theoretical and experimental evidence show that non-rectangular pulses are the most energy efficient waveforms for activating neuronal firings. Recently, non-rectangular waveforms and especially Gaussian signals have been studied for DBS due to their energy efficiency and neural stimulation performance [9]. But the effect of these non-rectangular waveforms on various target sites in the basal ganglia is not fully examined. Although designing the optimal energy efficient waveform is of great interest in many fields along with neuromodulation [51], minimizing the risk of tissue damage must be considered along with the pulse shape design. Non-rectangular DBS pulses have been used in analytical membrane models, however their impact on neural population models have not been fully investigated.

2.7   DBS waveform effects

Many studies have attempted to examine the therapeutic effect of DBS waveforms on patients with Parkinson's disease [21, 52, 53] along with more computationally based studies such as [3, 12, 14, 15, 22, 54]. However, the effect of DBS pulse modification with

a delay in a complex network of the basal ganglia has not been fully investigated. A typical waveform to be used as DBS is consisted of Cathodal pulse followed by a longer extent of an Anodal pulse [39]. In order to have a charge balanced wave, we must carefully define the cathodic to anodic pulse width ratio to guarantee enough time for the depolarization of the membrane potential to have the maximum efficiency of DBS. The main DBS waveforms used in literature are rectangular pulses, ramp, triangular and sinusoid [12]. All these waveforms are able to decrease the synchronization of GPe and GPi cells with a cathodic amplitude of 200 μA. The pulse duration of cathodic phases were 0.3 ms which is enough to elicit an action potential with minimum energy consumption [14] and for the anodic phase, the amplitude of -20 μA and duration of 1 ms was assigned. The delay of 0.7 ms shows a promising value for the activation of resting neurons in our basal ganglia network. These values are used in previous studies [3, 12, 14, 22] and showed relatively acceptable results. In terms of energy consumption of the DBS device, sinusoid pulse consumed the lowest amount of energy, suggesting that these signals can be beneficial in terms of battery loss and replacement surgeries.

Placing a delay between the cathodic and anodic phases had been studied by [15, 18] with only a rectangular pulse gap pulse waveform implemented on a simple Hodgkin-Huxley and a Morris-Lacar model, which does not consider the interactive behavior of the STN, GPe and GPi neurons [55]. They considered the effect of this DBS waveform by switching the cathodic and anodic phases, hence two waveforms of cathodic gap anodic (CGA) and anodic gap cathodic (AGC) were explored. The anodic phase must have lower amplitude with large duration to counter balance the effect of the short length but high

amplitude cathodic pulse. With this configuration, we can minimize the tissue damage of patients going under DBS implantation [56-58]. Interfering the DBS waveform with a delay between the cathodic and anodic parts also increases the threshold for the activation of neurons and will make the network less influenced by the anodic phase. Figure 2.5 shows a charge balanced biphasic rectangular pulse used in clinical settings for DBS.
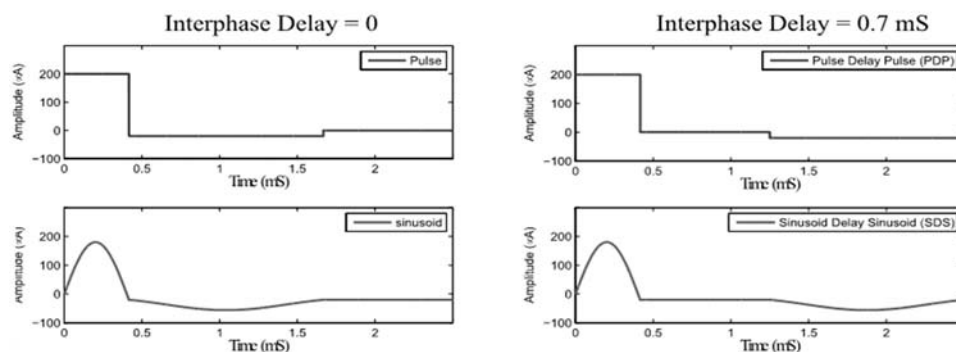
Figure 2.5 DBS waveforms without interphase delay (left) and with interphase delay (Right)

2.8   Closed Loop Deep Brain Stimulation

The schematic of open loop and closed loop DBS are shown in Figure 2.6. The therapeutic effects of DBS are enhanced once it is used in a closed loop paradigm. The cortical and pallidal discharge patterns of neurons are more improved by closed loop DBS rather than traditional open loop stimulations [59]. DBS is mainly targeted at subthalamic nucleus (STN) or globus pallidus externa (GPe) cells to disrupt the thalamo-cortical synchronizations seen in PD. Therefore, the local field potential (LFP) recorded from a population of the STN cells is often used as the feedback variable for DBS parametrization. Retrospective studies mainly focused on adjusting the stimulation amplitude based on the recorded LFP [18]. However, adapting the frequency of stimulation might provide superior results in desynchronizing the coupling patterns of

STN-GPe. Adjusting the frequency of stimulation to a protocol where HFS is only used when high desynchronization is needed, can expand the battery lifespan and reduces the necessity of costly battery replacement surgeries [60].
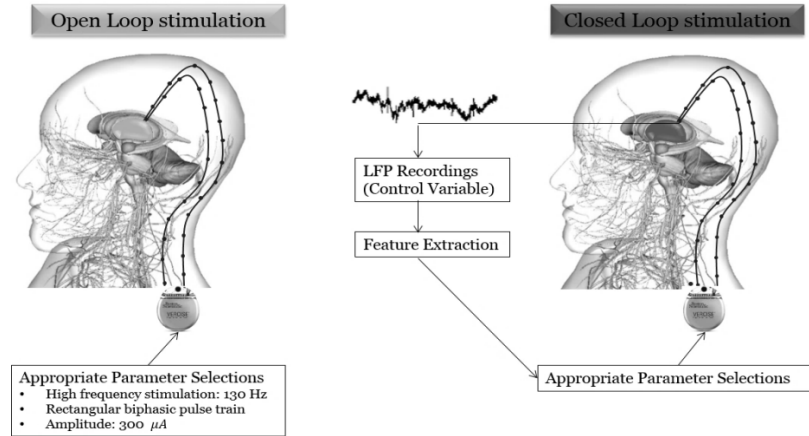
Figure 2.6 Open and closed loop paradigms for DBS in PD

It has been shown that closed loop DBS ameliorates akinesia and abnormal Cortico-BG discharges [59], improves therapeutic efficiency, increases battery lifespan, decreases tissue damage, and adjusts the oscillatory patterns [16, 41, 61, 62]. Closed loop models usually use the Local Field Potential (LFP) of the targeted region as the control variable since it is highly correlated with changes in the motor system [61, 63, 64]. LFP is then filtered and analyzed to be fed in a feedback algorithm. The decision of the feedback algorithm will set the next parameters for the DBS signal. For higher performance, the stimulation amplitude is reduced according to the amplitude of the filtered LFP signal [18]. Other studies compared linear and nonlinear feedback setups which yield different desynchronization results. Nonlinear feedbacks do not reinforce synchronization and act by compelling amplitude suppression of consecutive oscillations [65].

Due to the coupling dynamics of STN and GPe neurons, a synchronous burst firing is seen in the STN cells. This synchronized dynamic reflects a rhythmic activity in the STN neurons, which is observable from the LFP recordings and can be used to adjust the stimulation parameters. There are two approaches for closed loop DBS where both can optimize the stimulus signal to maintain a desired efficiency in terms of desynchronization as neuronal activities fluctuate. This is in contrast with open loop stimulation where a fixed HFS pulse train is applied to a target within the basal ganglia and in some cases, it causes tissue damage rather than alleviating the symptoms. The first approach for closed loop DBS defines a relationship between the measured output and the input stimulus. Since the stimulus is a function of the output (LFP) recordings only, other parameters such as the global interaction of cells with other regions of the brain are neglected. However, in delayed feedback closed loop DBS methods, the input stimulus is updated after the output recordings were put in a decision state. The decision state is where we define how to adjust the input stimuli according to the measured LFP signal for better therapeutic results. In this state, often one or a couple of parameters of the input stimulus are modified, considering more general features from the LFP signal such as power density of the recorded output and the oscillation frequencies.

To date, most of the delayed feedback algorithms focus on updating the amplitude of the stimulation signal according to the measured LFP. It has been shown that the power spectral density of the LFP signal can be used in a phase response curve (PRC) measure in order to deliver the stimulus signal at optimum frequencies [13]. In this method, using the subthreshold amplitudes for stimulation provided more compelling reduction of

pathological oscillations. However, stimulation with a burst of subthreshold amplitude increases the amount of energy consumed by the DBS device. In recent studies, the amplitude of the DBS signal was adjusted based on the damped filtered LFP signal and a gap was inserted between the phases of each DBS pulse. By this pulsatile feedback, the stimulation amplitude would have a linear relation with the filtered LFP. The advantage of this method is its ability to increase the battery lifespan while providing an adequate desynchronization [18]. Moving from adjusting the amplitude in feedback loops towards frequency adaptation might contribute to superior tradeoff between the desynchronization performance and the battery lifetime.

2.9   TMS and Neuronavigation Systems

TMS is a non-invasive protocol for activation of neurons in brain. It can generate magnetic fields over the scalp by applying a short electric current into the TMS coil. The schematic of a TMS coil along with the generated magnetic field are shown in Figure 2.7. TMS mostly activates the cortical parts of brain [66] and has shown to improve the therapy of major depression [67]. TMS is also effective for attention deficit hyper activity disorder, Schizophrenia and post-traumatic stress disorder.
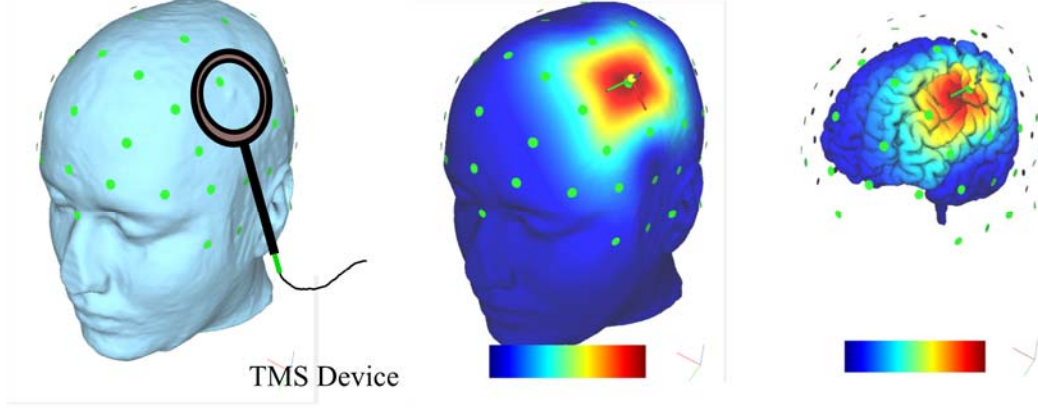
Figure 2.7 TMS device and simulated magnetic fields on the brain. TMS activation maps are run on SimNIBS.

The magnetic fields generated by TMS coils follow the Maxwell's equations as below [68]:

$$\nabla \bar{H} = j\omega \bar{D} + \bar{J} \qquad \text{while } \nabla \bar{D} = \rho \qquad (2.14)$$

$$\nabla \bar{E} = -j\omega \bar{B} \quad \text{while } \nabla \bar{B} = 0 \qquad (2.15)$$

In these equations, $\bar{H}$ is the magnetic field of a single TMS coil, $\bar{E}$ is the electric field, $\bar{B}$ is the magnetic induction and $\bar{D}$ is the electric induction. The charge and current densities are shown with ρ and $\bar{J}$ respectively [69].

The effects of these magnetic fields can be different from one subject to another due to the difference in size and shape of the human head. Many studies often tried to evaluate the effects of TMS on realistic head models [70, 71]. Recently a new quasi static boundary method was proposed, providing a real-time high-resolution stimulation tool [72]. Other studies have suggested multiple coils to stimulations to improve the therapeutic effects of TMS [73]. However, to achieve the optimal effects from TMS coils,

we need to move towards patient specific head models. There are several commercial and non-commercial software for MRI segmentation and head mesh generation such as Freesurfer [74], SimNIBS [75], Brain Voyager [76], etc . Although these software tools can generate reliable head meshes based on the MRI data of patients, they lack a robust algorithm to model abnormalities in the skull.

Ideally these models can be used for neuronavigation systems [68]. Neuronavigation is consisted of computer assisted technologies to navigate through brain regions [77]. The MRI data of each patient can be used to generate a 3D model of brain volumes and surfaces such as skin, skull, scalp, Cerebrospinal Fluid (CSF), White Matter (WM) and Grey Matter (GM). Physicians can navigate through these meshes and define the optimal targets for TMS therapy as shown in Figure 2.8. Similar 3D modeling approaches have been used for patient specific stimulation in DBS, estimation of gait posture and tDCS [44, 78-80].
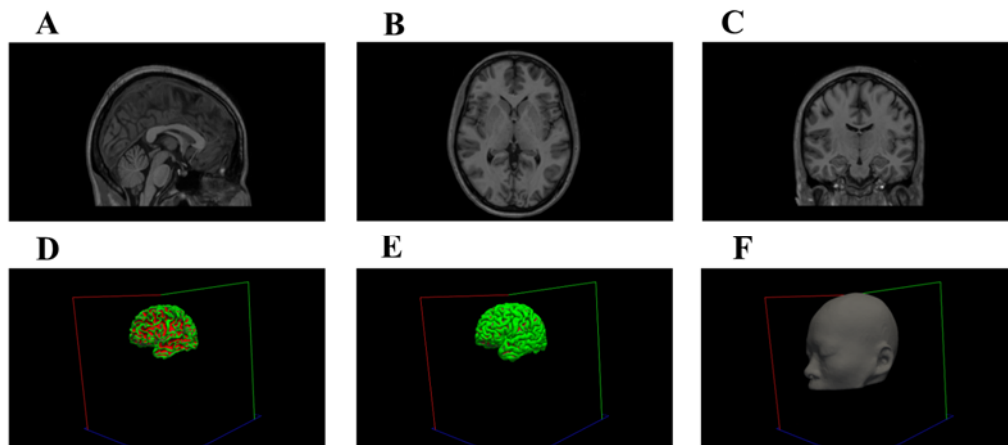
Figure 2.8 3D brain volume modeling from MR images. A) Sagittal view, B) Axial view, C) Coronal view. The generated WM, Pial surface and head mesh from MRIs are shown in D, E and F respectively.

2.10   Summary

Computational models of neuronal populations have been extensively used to investigate the underlying mechanism of DBS. Neuronal modelling has taken various approaches in terms of complexity, biological reliability and region of interest characteristics. Magnetic field models have also been used to study the effects of DBS on axonal activations and white matter pathways [44]. DBS method itself can be used in open loop, closed loop (Adaptive) or on demand paradigms. Table 2.1 summarize some of the relevant research articles in the field of DBS for PD.

Table 2.1 Summary of the literature research

Work	Methodology	Advantages	Disadvantages Cons
Rubin & Terman. 2004 [23]	Original Rubin and Terman (RT) model based on Hudgkin-Huxley equations.	Able to reproduce both pathological and physiological activities of STN, GPe, GPi and Thalamic cells.	Does not consider the effect of sensory motor cortex excitatory inputs.
Miocinovic et al. 2006 [10]	Electric field model of BG	Capable of analyzing axonal activations	STN dynamics showed discrepancy in terms of activations.
Pirini et al. 2009 [11]	Enhanced Rubin and Terman (RT) model with the effect of Striatum cells on the network and Rectangular DBS on different neuronal targets.	Representation of direct pathways of the basal ganglia cells.	Some phenomena like electrode to neuron distance, effects of somas, dendrites and axons, synaptic activation/inactivation effects, and neurotransmitter depletion are not considered by this work
Foutz & Mclntyre. 2010 [12]	Energy efficient non- rectangular DBS waveform	Examining the neuronal activation energy in both intracellular and extracellular stimulation.	Proposed waveforms are hampered by increased charge requirements, which may limit potential savings in battery life.
Wongsarnpigoon & Grill. 2010 [14]	Gaussian energy efficient DBS	Ability to find the optimal DBS waveform parameters	Lack of DBS targeting consideration.

	waveform with Genetic Algorithm	with the Genetic Algorithm	
Hofmann et al. 2011 [15]	Charge balanced DBS waveforms with introduction of a gap between cathodic and anodic phases	Modified DBS waveforms showed a considerably increased efficiency in terms of activation and entrainments of neuronal activities	Considering these DBS waveforms on a single compartment model rather than neuronal population network. Only considers rectangular pulses.
So et al. 2012 [3]	Enhanced RT model with rectangular DBS waveforms.	High ability to reconstruct the biological phenomena happening in the basal ganglia cells.	The model does not consider 3 dimensional orientations of different nuclei and the position of the stimulating electrode.
Priori et al. 2013 [63]	Adaptive analysis of LFP for closed loop stimulation	Showed LFP has correlation with motor and non-motor symptoms which makes it suitable as the control variable	Beta activity is not always detectable from LFP especially in rodent models
Summerson et al. 2015 [22]	Various charge balanced DBS waveforms implemented on a new cortical model.	High complexity and accuracy of model with considering the layer V into the model.	Irregular DBS waveform used does not provide the mean to understand the effect of DBS waveforms parameters.
Holt et al. 2016 [13]	Closed loop approach of Deep Brain Stimulation on the Hahn and McIntyre (HM) model	Considers the closed loop phasic stimulation which enables applying the DBS waveform at a proper time.	The complexity of neuronal network is not fully addressed by the model.
Popovych et al. 2017 [18]	Closed loop approach based on Rubin and Terman model	Showed that pulsatile stimulation can enhance the desynchronization process of pathological oscillations	Model is simplified and has neuroanatomy and neurophysiology limitations
Gunalan et al. 2018 [44]	Quantifying the axonal response due to DBS in a patient specific model	Provides insight into the modulated brain circuitry and possible correlations with clinical outcomes	The predictive capabilities of this model shows some limitations

CHAPTER 3: RESEARCH PLAN

3.1   Overview

As the first step of this work, we developed a low complexity model of single neurons [81]. This model can help realize the neuronal interconnection issues. The model can demonstrate various neuronal behavior observed in vivo through simple parameter modification. The behaviors include tonic and phasic spiking, tonic and phasic bursting, class 1 and class 2 excitability, rebound spike, rebound burst, sub threshold oscillation, accommodated spiking along with inhibition neuron responses. We investigate the neuronal spiking patterns in Parkinson's disease through our proposed model. We then compare this model with some of well know models [1, 2] to study the effect of DBS waveforms in terms of desynchronization of pathological oscillations and energy efficiency [9]. We also propose new Gaussian waveforms embedded with interphase delays, to increase the efficacy and efficiency of stimulation. This novel Gaussian waveform is used in a populational model of BG to investigate various targets for DBS. Additionally, we propose a 3 dimensional model based on the Izhikevich formulation [43]. Low cost computation of this model guarantees the simulation of large neuronal population. We also consider the synaptic connections within all neurons based on more realistic models to examine the synchrony in the Cortico-BG network along with LFP assessments. Our model

is able to generate the membrane voltages of the BG neurons, temporal firing patterns, and synchrony dynamics seen in experimental recordings [82]. This model is used to further test our novel closed loop (adaptive) stimulation protocol called Frequency Adjustment Stimulation (FAS) [25]. Our protocol adjusts the frequency of stimulation according to the level of synchrony observed by the LFP signal. For instance, HFS is only applied at the peaks of LFP signal where the synchronization is relatively high and the stimulation frequency declines as the synchronization level reduces. Closed loop adjustment of the frequency of stimulation shows better desynchronization while being energy efficient [3]. In addition, frequency adaptation has more therapeutic effects since various symptoms of PD correlate with different range of stimulation frequencies [27, 83].

Additionally, we proposed a new pipeline for TMS navigation to improve the quality of patient specific models while providing a tool for clinicians to better target and stimulate brain regions. The proposed pipeline is run by MATLAB software (Mathworks Inc.) with minimum system requirements of 2.7 GHz processor and 8 GB of memory.

3.2   Proposed Hyperbolic Model of Single Neuron

The Hyperbolic model can be used to study the neuronal firing patterns of cells with dopamine deficiency. This model is an extension over previously bi-dimensional models such as the Izhikevich model [2] and Adaptive Exponential Integrate and Fire (AdEx) model [84] which allows more flexibility by simply reducing the number of parameters in order to generate various spiking patterns. Due to the ambiguous nature of neuronal responses and the partial differential equations that can model them, we consider a hyperbolic differential equation to model all types of bursting behavior. This idea comes

27

from the vast applications of hyperbolic functions to solve differential equations. The proposed mathematical model can be formulated as follows:

$$\frac{dv}{dt} = \alpha \cosh\left(\frac{v-v_{rest}}{\beta} - 1\right) - \epsilon - H + I \qquad (3.1)$$

$$\frac{dH}{dt} = \tau_H(n_H v - H) \qquad (3.2)$$

We considered the insulation of cell membrane around a neuron as a capacitor which is defined by parameter α. Current I in this model represents the ionic movement through cell gates (inward Calcium and Sodium ionic velocity), resulting in action potential or voltage spikes. In existence of current I, the membrane voltage would increase and generate spiking patterns until it reaches a threshold value and should be reset to a resting state via v_{rest}. The sharpness of spikes can be modified through β. The ϵ parameter is an experimentally determined parameter, related to the general gate voltage of inward Calcium, Sodium and outward Potassium currents. Equation 3.2 can determine the rate of spikes along with their resting and peak times. Simply, by changing parameters in these equations, one can observe different types of neuronal firing. As shown in Figure 3.1, with the selection of $\alpha = 75000$, $\beta = 1000$, $v_{rest} = -62.5$, $\epsilon = 16$, $\tau_H = 0.02$, $n_H = 0.2$, we can see the tonic bursting behavior of neurons spiking. We tested a single tonic spike generated in our model (S_1) with the actual recordings of STN neurons (S_2) using the Cross Correlation (CC) measure as shown in Equation below.

$$CC(S_1, S_2) = \frac{\sum_{t=1}^{L}(S_1 - mean(S_1))(S_2 - mean(S_2))}{\sqrt{\sum_{t=1}^{L}(S_1 - mean(S_1))^2 \sum_{t=1}^{L}(S_2 - mean(S_2))^2}} \qquad (3.3)$$

L is the length of a spike, and as shown in Table 3.1, the hyperbolic model and AdEx models obtained the maximum CC values with actual recording of STN spikes [85].
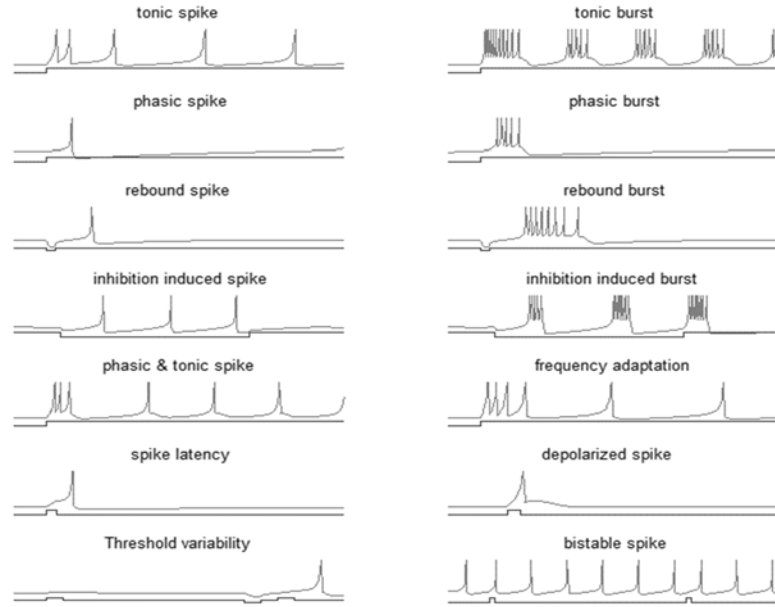
Figure 3.1 Different spiking patterns generated by Hyperbolic model

Furthermore, the hyperbolic model is able to generate switching firing patterns of STN neurons caused by Parkinson's Disease. This switching behavior from tonic to bust cannot be obtained by Izhikevich or AdEx. Physiologically inspired models can obtain slightly higher CC [34] but the large parameter set of these models will significantly reduce the computational performance in terms of simulation and upswing time (Table 3.1). In terms of number of parameters, the hyperbolic model has 5 parameters in total (excluding the reset potential). The number of parameters for Izhikevich and AdEx is 4 and 6, respectively. Figure 3.1 shows various types of single neuronal responses that can be generated by this model. The responses include tonic spikes, tonic burst, Phasic spike, phasic burst and etc.

Table 3.1 Comparison of Hyperbolic Model with Well-known Neuron Models

	Izhikevich [2]	AdEx [84]	Humphries et al [34]	Hyperbolic [81]
Number of Parameters	4	6	9	3 to 5
Simulation Time(s)	0.108	0.152	0.424	0.084
Upswing Time(s)	0.0014	0.0011	0.0034	0.0005
CC	0.785	0.809	0.813	0.827

Table 3.2 Parameters of Hyperbolic Model

Spiking Patterns	Parameters					
	α	β	v_{rest}	ϵ	τ_H	n_H
Single spike	75000	950	-62.5	16	0.021	0.2
Bursting spike	69000	1000	-61.5	16.1	-0.026	-1
Single to Burst switching	71000	965	-62.5	15.7	-0.02	-1
Constant Current	74000	1000	-55.5	16.6	0.1	0.25
Absence of Dopamine	75000	1000	-62	16.2	0.02	0.2
Presence of Dopamine	75000	1000	-62.5	16.9	0.1	0.36

3.3 BG Population Model to Investigate the Effects of DBS Waveforms

This model adopts the basic differential equations of cells by [1] in an interconnected manner to stimulate involving neurons in the basal ganglia such as the STN, GPe, GPi and Thalamic (Th) neurons. The governing equations for Th, STN, GPe and GPi neuron are as follows:

$$C_{Th}\frac{dV}{dt} = -I_L - I_{Na} - I_K - I_T - I_{GPi \to Th} + I_{SMC} \qquad (3.4)$$

$$C_{STN}\frac{dV}{dt} = -I_L - I_{Na} - I_K - I_{ca} - I_{T-}I_{GPe \to STN} + I_{DBS} + I_{bias} \qquad (3.5)$$

$$C_{GPE} \frac{dV}{dt} = -I_L - I_{Na} - I_K - I_{ca} - I_T - I_{STN \to GPe} + I_{GPe \to GPe} + I_{DBS} + I_{bias} \quad \text{(3.6a)}$$

$$C_{GPi} \frac{dV}{dt} = -I_L - I_{Na} - I_K - I_{ca} - I_T - I_{STN \to GPi} + I_{GPe \to GPi} + I_{DBS} + I_{bias} \quad \text{(3.6b)}$$

where the conductance values for Leaky, Sodium, Potassium and T-type low threshold

spiking currents are 0.05, 3, 5 and 5 $\frac{mS}{cm^2}$ and the equilibrium potentials are -70, 50, -75 and

0 mV, respectively. I_{SMC} is the sensory motor cortex current representing the effect of other

cells in the cortex on Th neurons. I_{SMC} is defined as the normal distributed pulse train with

frequency of 14 Hz and coefficient variance of 0.2 with each pulse having the amplitude

of 3 $\frac{\mu A}{cm^2}$ and duration of 5 ms, in order to generate the unordinary signal train of motor

cortex. $I_{GPi \to Th}$ represents the inhibitory currents from a GPi neuron to each Thalamic

neuron with the conductance of 0.17 $\frac{mS}{cm^2}$ and equilibrium potential of -85 mV. Conductance

values for Leaky, Sodium, Potassium, Calcium and T-type low threshold spiking currents

are 2.25, 37, 45, 2 and 0.5 $\frac{mS}{cm^2}$ and the equilibrium potentials are -60, 55, -80, 140 and 0

mV, respectively. $I_{GPe \to STN}$ represents the inhibitory currents from 2 GPe neurons to each

STN neuron with the conductance of 0.5 $\frac{mS}{cm^2}$ and equilibrium potential of -85 mV. I_{bias} is

set to 29 $\frac{\mu A}{cm^2}$ for the healthy case and 20 $\frac{\mu A}{cm^2}$ for the Parkinsonian case and finally, I_{DBS} is

the deep brain stimulus used in the model. Conductance values for Leaky, Sodium,

Potassium, Calcium and T-type low threshold spiking currents are 0.1, 120, 30, 0.15 and

0.5 $\frac{mS}{cm^2}$ and the equilibrium potentials are -65, 55, -80, 120 and 0 mV, respectively and

these values are the same for GPe and GPi neurons. $I_{STN \to GPe}$ represents the excitatory

currents from 2 STN neurons to each GPe neuron with the conductance of 0.15 $\frac{mS}{cm^2}$ and

equilibrium potential of 0 mV. $I_{GPe \rightarrow GPe}$ represents the inhibitory currents from 2 GPe neurons to each GPe neuron with the conductance of 0.5 $\frac{mS}{cm^2}$ and equilibrium potential of -85 mV. $I_{STN \rightarrow GPi}$ represents the excitatory currents from 2 STN neurons to each GPi neuron with the conductance of 0.15 $\frac{mS}{cm^2}$ and equilibrium potential of 0 mV. $I_{GPe \rightarrow GPe}$ shows the inhibitory currents from 2 GPe neurons to each GPi neuron with the conductance of 0.5 $\frac{mS}{cm^2}$ and equilibrium potential of -85 mV. I_{bias} is set to 20 $\frac{\mu A}{cm^2}$ for the healthy case and 8 $\frac{\mu A}{cm^2}$ for the Parkinsonian case in Equation 3.5 and 22 $\frac{\mu A}{cm^2}$ for the healthy case and 12 $\frac{\mu A}{cm^2}$ for the Parkinsonian case in Equation 3.6.

Each GPe cell has inhibitory projections to two STN, GPi and GPe neurons while each STN neuron has 2 excitatory connections to two GPe and two GPi neurons, as shown in Figure 3.2. GPi neurons act as an output connection to Thalamic neurons with 1 inhibitory connection. This model also considers an irregular frequency pulse train as an input to the thalamic cells, exemplar of the accumulated current from the sensory motor cortex region. Many studies have attempted to examine the therapeutic effect of DBS waveforms on patients with Parkinson's disease [21, 52, 53] along with more computationally based studies such as [3, 12, 15, 18, 22]. However, the effect of DBS pulse modification with a delay in a complex network of the basal ganglia has not been fully investigated. A typical waveform to be used as DBS is consisted of Cathodal pulse followed by a longer extent of an Anodal pulse [39].
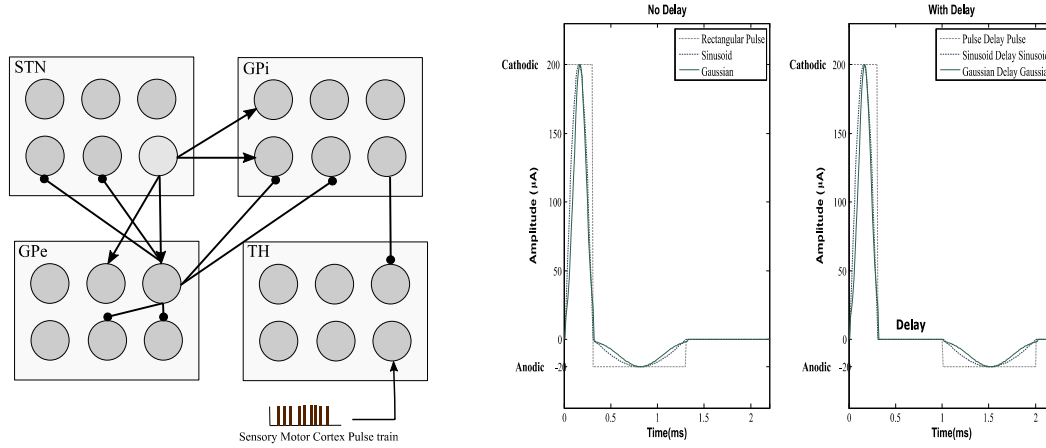
Figure 3.2 BG network model and various DBS waveforms

In order to have a charge balanced we must carefully define the cathodic to anodic pulse width ratio which in our study we set this ratio to 1:3.3 to guarantee enough time for the depolarization of the membrane potential to have the maximum efficiency of DBS. We compared a group of waveforms with a delay between the Cathodic and Anodic phases in the computational network of the basal ganglia to see how these DBS signals can activate the resting neurons along with the reduction of neuronal synchronization. These signals are rectangular pulses, sinusoid and Gaussian along with 3 biphasic waveforms with a delay between the cathodic and anodic parts, which we call Pulse Delay Pulse (PDP), Sinusoid Delay Sinusoid (SDS) and Gaussian Delay Gaussian (GDG) waveforms. All these waveforms were able to decrease the synchronization of GPe and GPi cells with a cathodic amplitude of 200 μA, pulse duration of cathodic phases were 0.3 ms which is enough to elicit an action potential with minimum energy consumption [14] and for the anodic phase the amplitude of -20 μA and duration of 1 ms was assigned. The delay of 0.7 ms showed a promising value for the activation of resting neurons in our basal ganglia network. We defined our DBS signals in the form of a cathodic phase followed by a delay and then

33

followed by an anodic phase. With this configuration, we were able to achieve the activation of resting neurons while having a fixed optimum delay length. The effect of a Gaussian delay Gaussian waveform has not been studied before which we showed is the most practical waveform for deep brain stimulation in terms of energy consumption, desynchronization of GPe/GPi cells and performance of proper elicitation of action potential within the network. Figure 3.2 shows the waveforms we used in the computational basal ganglia model.

3.4   Proper DBS targets for PD symptoms

Retrospective studies show that DBS targeting must be selected based on the patient's condition. In order to restore the thalamic relay activity, STN-DBS has the highest functionality, while GPe-DBS might inhibit the thalamocortical relay activity [86]. STN-DBS increases the risk of dyskinesia, and therefore should not be used for patients with L-dopa induced dyskinesia. It is known that the motor functionality of patients with STN-DBS and GPi-DBS increases, and symptoms such as tremor, rigidity and dyskinesia improve gradually under both STN and GPi DBS surgeries [87]. In recent studies, the GPe-DBS has shown higher effect in treating bradykinesia and akinesia than GPi-DBS [88]. Due to PD, the neural activity in the nuclei of the basal ganglia neurons changes in terms of mean firing rate and discharge patterns. We discuss the effect of Gaussian DBS signals applied to different targets with three metrics: Average Action Potentials (AAPs), Synchronization Level (SL) and Energy Consumption (EC).

3.4.1   Average Action Potentials (AAPs)

Using a threshold of -20 mV, the Action Potentials (APs) of neurons is calculated and the average of these APs is obtained for 1000 GPi neurons in our model. The reason for measuring only the AAPs of GPi neuron is that the GPi neurons provide inhibitory input to the Th neurons, which is considered as the output of the model. In addition, alteration in GPi firing pattern is directly associated with symptoms of PD [89].

3.4.2 Synchronization Level (SL) and Energy Consumption (EC)

There are several methods to measure the level of synchrony with the neuronal population [9, 11, 17] or . Here, we measure the extent of synchronization by considering the order parameters based on the aggregated phases of all neurons [90]. Based on this method, measuring the Synchrony Level *SL(t)* would be more comprehensive, since the phases of neurons define the extent of synchrony.

$$SL(t) = |\frac{1}{N}\sum_{n=1}^{N} e^{i\rho_n(t)}| \qquad (3.7)$$

$$\rho_n(t) = 2\pi(t - t_b)/(t_{b+1} - t_b) \qquad (3.7a)$$

$\rho_n(t)$ denotes the phases of each neuron and t_b is the onset time of the bth burst [18]. *SL(t)* ranges from 0 to 1 indicating no or full synchrony. The total amount of Energy Consumed (*EC*) by the whole DBS protocol can be described by [90]:

$$EC = N_{P_{bi}} \int I_{DBS}(t)dt \qquad (3.8)$$

$N_{P_{bi}}$ is the total number of pulses used in $P_{bi}(t)$. The more pulses are applied (HFS), the more energy is consumed and since our protocol only applies HFS under high synchronization, we expect less *EC* value compared to amplitude modulation methods [16, 18].

3.5   Adaptive Frequency Adjustment Stimulation

3.5.1   BG 3D Model

We proposed a 3 D model of basal ganglia neurons based on Izhikevich formulation [43]. The schematic of the model is shown in Figure 3.3. Each nucleus has a population of 125 neurons with their interconnections [91]. These neuronal subpopulations are aligned in a 5×5 symmetric cubic space, as shown in Figure 3.3.
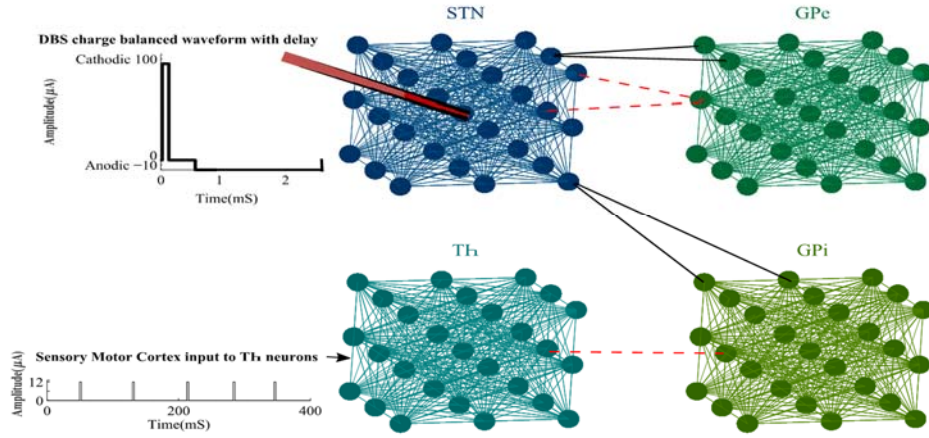
Figure 3.3 The 3D network of BG neurons

Each STN neuron has excitatory connections to 2 GPe and 2 GPi neurons. GPe neurons have inhibitory connections to 2 STN neurons and finally, there is one inhibitory synopsis from each GPi to a Th neuron [42]. We considered a local field of connections between all pairs of neurons within each nucleus (Figure 3.3), to match the local connectivity developed by hippo-campus studies [92].

It has been shown that glutamatergic synapses exist in the STN neurons [93], the connections of Globus Pallidus neurons are mediated by $GABA_A$ receptors [94, 95] and

36

local interneuron synapses control the Thalamic circuitry [50]. Therefore, we considered the excitatory coupling between neurons in each subpopulation which is overlooked in many computational models of the BG [14, 18, 96]. These synaptic connections within each nucleus were obtained by the following equation as a function of the membrane and resting state voltages V^j and E_S^j, respectively.

$$I_S^j = g_S(V^j - E_S^j) \sum_{i=1}^{N} W_{ij}S_S \qquad (3.9)$$

where I_S^j is the total synaptic currents from all neurons of a specific nucleus to neuron j. The membrane conductance g_S was set to 1.5, 3.5, and 10 for the Th, STN, and GP populations, respectively, to assure the desired connections. In order to reflect the strength of the connections within each nucleus, we account the synaptic weights W based on the distance between each pair of neurons. Therefore, $\sum_{i=1}^{N} W_{ij}$ in Equation 3.9 denotes the sum of all weights from N neurons in the population to neuron j. These weights were measured as follows.

$$W_{ij} = e^{\frac{-\|n_i - n_j\|^2}{2\sigma^2}} \qquad (3.10)$$

In Equation 3.10, $\|n_i - n_j\|^2$ is the Euclidean distance between neuron i and neuron j. The parameter σ was set small to ensure that relatively far neurons receive weak and negligible connections from each other as opposed to primary projecting neurons and interneurons, where stronger connections are needed. The synaptic dynamic S_S in Equation 3.9 was defined by a first order process to reduce the computational cost of a large network.

$$\frac{dS_S}{dt} = -\alpha_S S_S + \delta(t - T) \qquad (3.11)$$

where α_S and T represent the reverse potential and the time of presynaptic spikes, respectively [97]. The excitatory and inhibitory synapses between different BG cells were defined by Equation 3.12. S_j in this equation stands for the summation of all presynaptic dynamics. In case of inhibitory connections from GPe to STN, S_j consists of 2 presynaptic currents, while S_j would have only one presynaptic current for the GPi-Th connections.

$$I_{syn}^{i \rightarrow j} = g_{ij} S_i (V^j - E_{syn}^j) \qquad (3.12)$$

We also considered a random pulse train I_{SMC}, modeling the aggregated inputs from sensory motor cortex to Th (Figure 3.3). The amplitude of this current was set to 12 μA with pulse width of 2.8 mS. After general initialization of our BG model, the governing membrane voltage equation for each neuron type was achieved by an extension over the Izhikevich spike formulations [2] as below:

$$\frac{dV_{Th}}{dt} = 0.04 V_{Th}^2 + 5 V_{Th} + 140 - u_{Th} + I_S^{Th} + I_{SMC} - I_{syn}^{GPi \rightarrow Th} \qquad (3.13)$$

$$\frac{dV_{STN}}{dt} = 0.04 V_{STN}^2 + 5 V_{STN} + 140 - u_{STN} + I_S^{STN} + I_N^{STN} - I_{syn}^{GPe \rightarrow STN} + I_{appSTN} + e^{-D} I_{DBS} \qquad (3.14)$$

$$\frac{dV_{GPe}}{dt} = 0.04 V_{GPe}^2 + 5 V_{GPe} + 140 - u_{GPe} + I_S^{GPe} + I_N^{GPe} + I_{appGPe} - I_{syn}^{STN \rightarrow GPe} \qquad (3.15)$$

$$\frac{dV_{GPi}}{dt} = 0.04 V_{GPi}^2 + 5 V_{GPi} + 140 - u_{GPi} + I_S^{GPi} + I_N^{GPi} + I_{appGPi} - I_{syn}^{STN \rightarrow GPi} \qquad (3.16)$$

$$\frac{du}{dt} = a(bV^2 - u) \qquad (3.17)$$

The term e^{-D} in Equation 3.14 provides an exponentially debilitating effect on how each neuron is influenced by the DBS current, where D is the Euclidean distance between

the neuron and the electrode. u_{STN} incorporates an Ordinary Differential Equation ODE such as Equation 3.17 with different adjusting parameters stated in Table 3.3.

Table 3.3 Parameters of 3D BG Model

	α_S	a	b	c	d	$I_{app}(\mu A)$
Th	0.5	0.02	0.2	-65	5	0
STN	0.5	0.01	0.27	-65	8	1
GPe	0.3	0.2	0.26	-65	0	0.2
GPi	0.3	0.2	0.26	-65	0	0.3
Synaptic Currents	$g_{GPe \to STN}$ = 1.5	$g_{STN \to GPe}$ = 2.5	$g_{GPe \to GPe}$ = 1.5	$g_{STN \to GPi}$ = 2.5	$g_{GPi \to GPi}$ = 1.5	$g_{GPi \to Th}$ = 2.3
	$E_{GPe \to STN}$ = -85	$E_{STN \to GPe}$ = 0	$E_{GPe \to GPe}$ = -65	$E_{STN \to GPi}$ = 0	$E_{GPi \to GPi}$ = -65	$E_{GPi \to Th}$ = -65

3.5.2 FAS Protocol

Rhythmic oscillation of the STN neurons interacting with the GPe cells has been observed in PD [98]. This rhythmic nature can be captured by the LFPs of STN neurons. We used the same location as the DBS electrode was targeted to measure the LFP of the STN neurons according to the following Equation [18, 99].

$$LFP_{STN}(t) = \frac{R}{4\pi} \sum_{i=1}^{N} \frac{I_{STNi}(t)}{D_{ic}} \qquad (3.18)$$

where R is the extracellular resistance set to 1, assuming to be homogenous throughout the population. D_{ic} is the Euclidean distance between neuron i and the center of population where the LFP recording electrode is placed (Figure 3.3). $I_{STNi}(t)$ is composed of all currents on the left hand side of Equation 3.13-3.16 for the ith STN neuron. The LFP signal is then filtered using a damped oscillator as follows.

$$\ddot{x} + \omega\dot{x} + \omega^2 x = K_S LFP_{STN}(t) \qquad\qquad (3.19)$$

where ω denotes the frequency of oscillation and is approximated at $62\,\frac{rad}{sec}$ since the period of each oscillation is around $100\,mS$ ($\omega = \frac{2\pi}{T}$). K_S is a scaling coefficient set to 0.01 in this filter. The output of the damped oscillator is often delayed due to the filtering process. Thus, the feedback stimulator signal $FS(t)$ is defined by shifting $\dot{x}$ by half of the period of oscillation. This is essentially a linear delayed feedback used in closed loop stimulations [100].

$$FS(t) = I_{DBS}(KLFP_m(t)t) \qquad\qquad (3.20)$$

$$LFP_m(t) = \dot{x}\left(t - \frac{T}{2}\right) - \dot{x}(t) \qquad\qquad (3.20a)$$

where $LFP_m(t)$ is the filtered and delayed LFP signal. $T = \frac{\omega}{2\pi}$ is the period of oscillation and K is the feedback gain set to 2. The $FS(t)$ acts as a linear delayed feedback control to adjust the frequency of the stimulation signal I_{DBS}. We introduce a Frequency Adjustment Stimulation (FAS) method in our work to be able to alter the frequency of stimulation based on the amplitude severity of the filtered LFP signal. Generally, high peaks of $\dot{x}(t)$ denote higher synchronization and HFS has been proven to have better efficiency in desynchronization [101]. However, continuous HFS increases the risk of tissue damage while decreasing the battery lifetime [102, 103]. The FAS in our proposed method tends to send HFS during the peak of $\dot{x}(t)$ and slightly decrease the frequency of stimulation as the peak of $\dot{x}(t)$ descends. This allows for enhancing the synchronization process while addressing tissue safety concerns. The amount of energy consumed by the

DBS device is reduced since HFS is only used for short periods of $\dot{x}(t)$ peaks. Lower energy consumption reduces the need for costly battery replacement surgeries. In addition, variant stimulation frequencies have been shown to have different therapeutic effects based on the symptoms of the patients [104, 105]. The schematic of the delayed feedback loop with the proposed FAS protocol is shown in Figure 3.4.
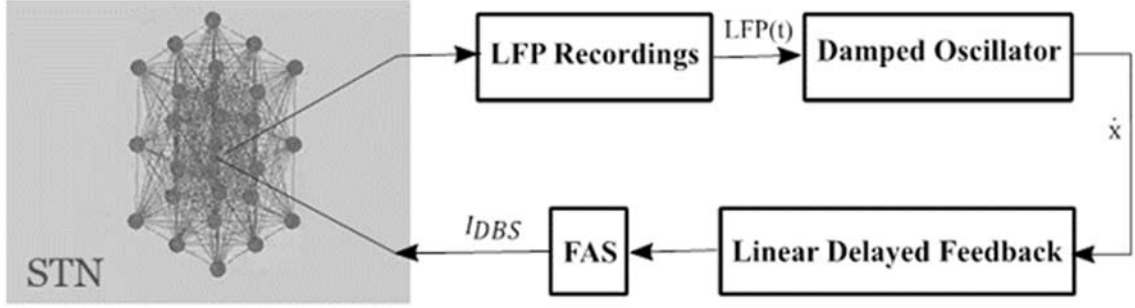
Figure 3.4 Closed loop (Adaptive) paradigm for FAS method

3.6 Neuronavigation TMS Pipeline

Here, we propose a new pipeline for navigated TMS systems. The goal is to generate a 3D volume of the brain regions from the individual MRIs and measure the magnetic field on these 3D models. This allows physicians to go through various areas of the brain to define proper targets for TMS fields. Additionally, TMS effects can be measured by the Electromyography (EMG) potentials which can help physicians better localize and stimulate with the TMS device [68, 106]. Trackers on the TMS provide real-time tracking of the coil coordinates [107]. The combination of TMS coil coordinates and EMG is often used to improve the quality of cortical maps in neuronavigation systems [108]. The schematic of the proposed neuronavigation TMs pipeline is shown in Figure 3.5.
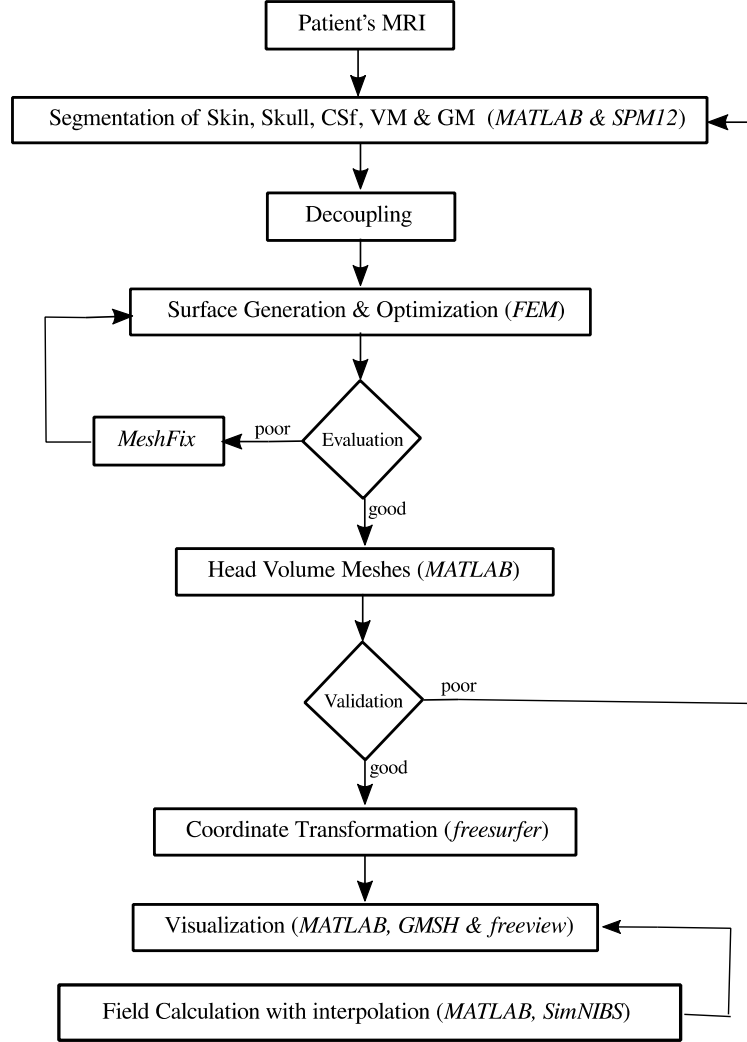
Figure 3.5 The proposed pipeline for the neuronavigation TMS systems.

At first, the structural MR images of each patient are used to segment the brain volumes. For these segmentations we used an extended tissue probability mapping based on [109]. We used tissue probability maps to get the spatially varying prior distributions [110]. Then, the probability of class/tissue k at the voxel i is measured by:

$$P(c_i=k/\gamma)= \frac{\gamma_k b_{ik}}{\Sigma_{j=1}^{k}\gamma_j b_{ij}} \qquad (3.21)$$

Where γ represents the weight and b_{ij} is the value of the jth tissue probability at voxel i. Once all tissues (skin, skull, CSF, WM, GM) were segmented, we decouple them with the assumption that subsequent surfaces are fully contained within each other [71]. The next step is to generate and optimize surfaces using adaptive meshing [111]. Furthermore, we used 2 metrics to evaluate the generated tetrahedral meshes. The Signed Inverse Condition Number (SICN) which measures the sensitivity and uncertainty of meshes to small changes or errors of input data [112-114] and Gamma test which measures the quality of inscribed and circumscribed radiuses [114], are performed.

As shown in Figure 3.5 if there are errors found after the surface meshing step, MeshFix [115] will modify the 2D tetrahedral meshes and new surfaces will be generated. In the next step, the 2D surface meshes are transformed into 3D volume meshes. In order to validate the volumes, we defined a set of points on a specific brain region such as skull on the MR T1-weighted images and checked the distance between these points and the actual segmented volume by the equation below:

$$l= \hat{n}x_0 - |proj_v - w| \qquad (3.22)$$

where $\hat{n}$ is the unit norm of the shortest vector to the surface, x_0 is the normal vector and $|proj_v - w|$ represents the projection of a plane vector w onto v. After validating meshes, we calculate the magnetic field of TMs coils by equations 2.14 and 2.15. The center of each coil is the coordinate used for field modeling. These voxel coordinates are then transformed to continuous coordinates using the Freesurfer software [116] as following:

$$Vox2ras = \begin{bmatrix} [x] & [y] & [z] & [c] \\ 0 & 0 & 0 & 1 \end{bmatrix}$$
(3.23)

Where x, y and z are 3×1 vectors defining the direction cosine which provides the orientation of the image volume in real space [117]. The modules of navigated TMS pipeline are mostly run on MATLAB. However, for visualization of results we can use other software tools such as Freeview [74], GMSH [114] or MATLAB.

CHAPTER 4: IMPLEMENTATION AND TESTING

All the proposed neuronal models were developed and tested in MATLAB software. We used a set of mathematical methods for testing each proposed contributions as follows: For the hyperbolic model proposed, we measured the number of firings under various conditions and compared it with experimental recordings as shown in Table 3.2. The irregular firing patterns of PD are generated by the model and compared with the LFP recordings of monkeys. As shown in Equation 3.3, cross correlation is used for comparison of the results with other methods.

Stimulation waveform effects were investigated through synchrony analysis (Equation 3.7). Additionally, we measured the amount of energy consumed by each stimulation waveform according to Equation 3.8. We investigated the effect of interphase delay on the amount of energy consumed by simply increasing the delay length and measuring the total energy usage of the DBS protocol. Mutual Information (MI) and Phase Locking Values (PLV) methods were also used as metrics of evaluating the amount of pathological oscillations as below:

$$MI(Y_H, Y_{DBS}) = \sum_{i=1}^{M} \sum_{j=1}^{M} P_{Y_H Y_{DBS}}^{ij} \ln\left(\frac{P_{Y_H Y_{DBS}}^{ij}}{P_{Y_H}^{i} P_{Y_{DBS}}^{j}}\right) \qquad (4.1)$$

where $P_{Y_H Y_{DBS}}^{ij}$ is the estimated joint probability of the outcomes i and j for the signals and $P_{Y_H}^{i}$ is the estimated probability distribution of the ith outcome of Y_H.

For PLV analysis, first of all, we must extract the instantaneous phases from the signals

using a Hilbert transform as below:

$$\varphi_Y = \tan^{-1}(\frac{H(Y)}{Y}) \qquad (4.2)$$

where $H(Y)$ is the Hilbert transform of signal Y. In order to see how well the firing

patterns of STN, GPe and GPi neurons under DBS (Y_{DBS}) is phase locked to the healthy

condition (Y_H), we can use the following measure:

$$\text{PLV}(Y_H, Y_{DBS}) = \frac{1}{L}\left|\sum_{i=1}^{L} e^{j\left(\varphi_{Y_H}-\varphi_{Y_{DBS}}\right)}\right| \qquad (4.2)$$

We tested the desynchronization efficiency of various DBS targets by correlation

coefficient analysis. Correlation coefficient analysis based on the desired APs can be a

metric to measure the synchronization level among GPi neurons. For the population of

1,000 GPi neurons, we extracted the number of APs for each non-overlapping frames of

10 mS. This provides a function of the number of APs based on each frame for every GPi

neuron. Equation 4.4 shows the number of APs for neuron i in l consecutive frames:

$$F_i(I) = \sum_I AP \qquad (4.4)$$

Then, the correlation coefficients of 1,000 F_i functions are calculated from

Equation below:

$$CC(F_i, F_j) = \frac{\sum_{t=1}^{L}(F_i - \overline{F_i})(F_j - \overline{F_j})}{\sqrt{\sum_{t=1}^{L}(F_i - \overline{F_i})^2 \sum_{t=1}^{L}(F_j - \overline{F_j})^2}} \qquad (4.5)$$

L is the number of elements in each function. For GPi population of 1,000 neurons, a

1,000 by 1,000 elements correlation matrix M_C between all GPi neurons is generated

using Equation 4.5. The total number of values in matrix M_C with significant correlation

($\alpha \leq 0.05$) is called n_c, while the total number of elements in M_C is denoted by n_τ. The

synchronization level (SL) for the GPi neurons is finally derived by the Equation below:

$$SL = \frac{n_c}{n_r} \qquad (4.6)$$

The FAS method: We used Equations 3.13-3.16 to implement the 3-D Volumetric

Model in MATLAB. The firing patterns of all neuronal types were extracted and the

measured LFP signal was used for the FAS protocol. Additionally, with Fourier transform

we measured the Power Spectral Density of STN-LFPs under various stimulation

protocols. Furthermore, we investigated the effect our proposed FAS method on large

neuronal population model.

CHAPTER 5: RESULTS

5.1   Simulation of the Hyperbolic Model

STN Neurons show three different types of firing patterns: bursting, irregular and rhythmic. The bursting patterns usually occur with high frequency spikes, which in humans would vary from 18 to 28 spikes per seconds [118]. Irregular patterns are considered as randomly rapid inter spike firings. Finally, the rhythmic patterns generate single spikes with multiple peaks. It is shown by the measurement of STN spiking that both tonic and burst patterns exist [85]. Based on the current value of membrane potential, STN neurons can change their firing patterns from single spike mode to bursting patterns. This transition between two modes is observed via our mathematical model. Recordings of STN neurons spikes reveal that the single spike peak is between -35 to -70 mV and burst spikes generate the membrane potential of -42 to -60 mV [85].
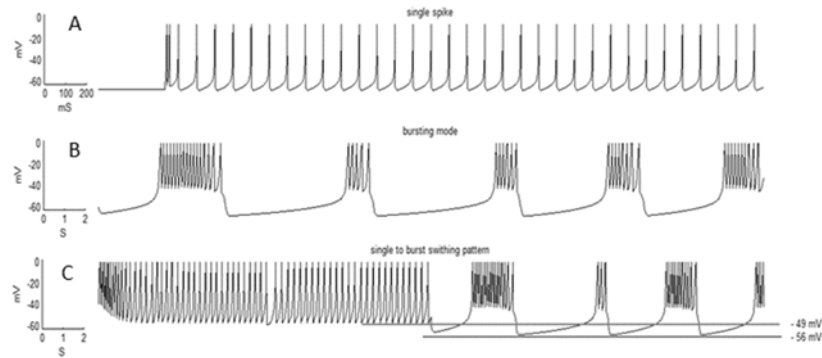

Figure 5.1 Single, burst and switching mode of STN neurons spiking generated by the proposed Hyperbolic Model.

Figure 5.1 shows single spiking, burst spiking and the switching pattern from single spikes to burst spikes generated by our model using MATLAB. Scientists believe that there

48

is a relation between excessive bursting patterns in STN neurons and Parkinson's disease [119]. The important question now is how the firing patterns of STN neurons, considering their apparent features, are related to Parkinson's disease. Generally, Parkinson's disease is accompanied by loss of dopamine innervation, leading to abnormal burst firing patterns in STN neurons. Researchers explained that dopamine may suppress synoptically triggered burst firing patterns, in the meantime, this suppression of burst firing patterns could be a result of a synaptic current.
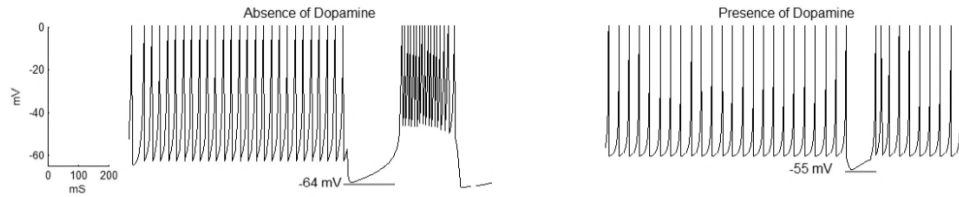
Figure 5.2 Absence (left) and presence (right) of dopamine in STN neuronal firing

In Figure 5.2, we modified our model to obtain both firing patterns of STN neurons in presence and absence of dopamine which has been recorded in related works [120]. The absence or presence of dopamine in our model is defined by parameters τ_H and n_H which represent the decay rate and sensitivity of spikes, respectively. τ_H is set to 0.02 and 0.1 to model the absence and presence of dopamine in STN neurons respectively. τ_H is much lower in the case of dopamine depletion compared to when dopamine is present which provides a faster decay time. Also, n_H is set lower for absence of dopamine in comparison with the presence of dopamine condition. This n_H parameter modification in case of dopamine depletion along with faster decay time due to low value of τ_H guarantees enough time for the transition of tonic spiking into burst firing patterns. In the presence of

dopamine, the transition is almost diminished, providing a more tonic pattern (Figure 5.2) due to higher values of τ_H and n_H.

5.2   Therapeutic Effects of Novel DBS Waveforms

We applied different pulse shapes as deep brain stimulators to investigate the energy consumed along with the number of times that the DBS signals failed to elicit an action potential by using Equation 3.8. We used the basic pulse, Sinusoid and Gaussian [14] waveforms and compared them to the modified waveforms with a delay between the cathodic and anodic phases, called Pulse delay Pulse (PDP), Sinusoid delay Sinusoid (SDS) and Gaussian Delay Gaussian (GDG). From the recording of the neuronal firing rates in monkeys [119, 121, 122], we expect to see an increase in the firing rate of GPi and STN after implementing the DBS signals, while GPe neurons show the reduced firing rate. In Figure 5.3, the mean firing rate of STN, GPe and GPi cells increased from PD condition to DBS implemented condition. From Healthy to PD condition, a decrease in the rate of GPe neurons is observable which is consistent with the recording data [3]. All six DBS waveform types successfully increased the rate of spiking in Thalamic, STN, GPe and GPi cells but the amount of this boost in neuronal firing was lower for GPe neurons while being stimulated by a GDG waveform, which promises better results in diminishing the effects of Parkinson's disease [122]. The relative increase in firing rates of GPe and GPi cells from PD to DBS implemented condition was corresponding to the experimental recordings in which the GDG and PDG waveforms in our model reached the highest comparability to the actual data [21].
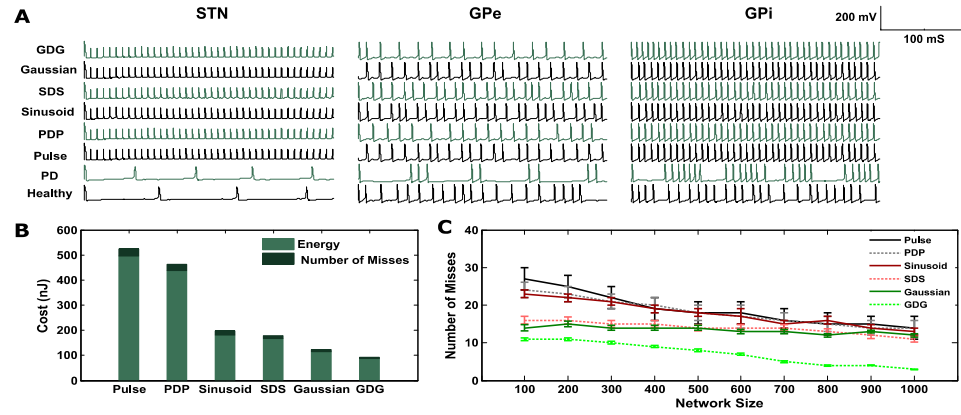
Figure 5.3 Cost evaluation of various DBS waveforms

Synchronization of brain waves is the basis of functional connectivity for neural decoding [123]. There are several bivariate techniques to study the synchronization in firing patterns of brain cells [124], namely, the mutual information, phase locking and synchronization levels based on the correlation coefficient [11]. STN, GPe and GPi neurons fire with various patterns under different DBS waveforms, therefore the similarity and synchronization of these firing responses compared to the firing pattern of these neurons under healthy condition is investigated by Mutual Information (MI) and synchrony Level (SL) as shown in Figure 5.4.
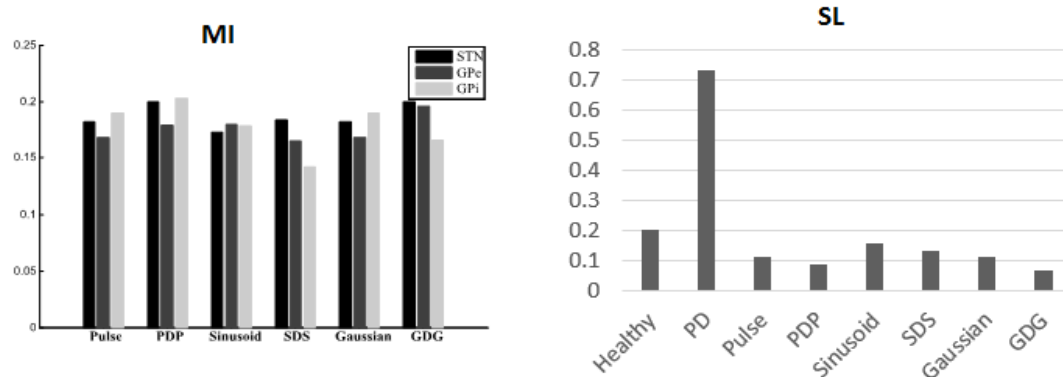
Figure 5.4 MI and SL values under different stimulation waveforms

The GDG was able to decrease the cathodic amplitude for eliciting an action potential because the cathodic Gaussian waveform will depolarize the membrane of the basal ganglia cells while the gradual decrease of the following anodic Gaussian phase will act as an extra delay for the depolarization process creating a less sensitive waveform to the anodic phase (Figure 5.5A). The GDG waveforms reached the delay threshold faster than SDS and PDP. In this figure, the duration of the anodic phase is 3.3 times of the cathodic phase and the ratio of the cathodic to anodic phases are set to 10:1. The threshold of the delay to reach the amplitude of 200 μA, capable of eliciting action potentials was 0.32, 0.43 and 0.65 mS with respect to GDG, SDS and PDP waveforms. The obtained cathodic amplitude to elicit action potential for PDP waveform was 30% lower than previous studies [3], while SDS and GDG had even lower amplitudes than PDP. The optimal values for these waveforms are shown in Figure 5.5B. GDG had the lowest cathodic amplitude while being able to function with relatively lower amplitude of the anodic phase compared to the SDS waveform (-19 μA for GDG anodic and -23 μA for SDS).
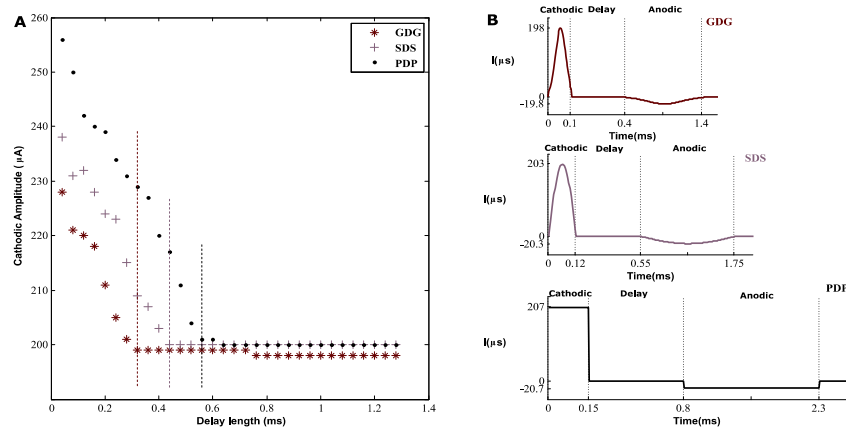
Figure 5.5 Optimal amplitude of DBS waveforms with respect to the delay length

We replaced the Hodgkin-Huxley formulation with Izhikevich and Hyperbolic and compared the cost as we increased the network size. Network size in Figure 5.6 represents the number of neurons in each nuclei. As we reach large networks, hyperbolic outperforms both Izhikevich and Hodgkin-Huxley models.
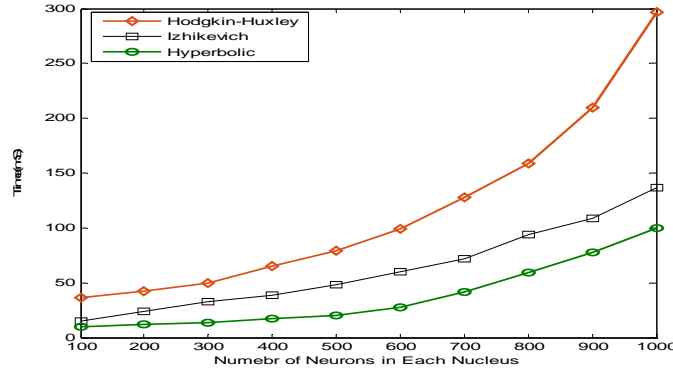
Figure 5.6 Energy consumption of different neuronal population models with respect to the network size.

5.3   Discussion of DBS Targets

We investigated the average firing rates of STN, GPe and GPi neurons under 3 different conditions (STN-DBS, GPe-DBS and GPi-DBS), as shown in Table 5.1. In this table, we compared the results of Gaussian DBS with rectangular pulses. It can be observed that both Gaussian and rectangular DBS signals performed similar in terms of firing patterns. The AAPs shown in this table is obtained over a firing period of 1s of GPi neurons. AAPs under STN-DBS were higher for all neuron types compared to GPe-DBS and GPi-DBS. This explains the high desire to target STN under DBS for PD patients with tremor, rigidity and bradykinesia [48]. Although GPe-DBS provides the lowest amount of AAPs for all neurons, it can be used for patients with akinesia [125].

Table 5.1 AAPs of Basal Ganglia Neurons

DBS Signal Form	DBS Target	AAPs		
		STN	*GPe*	*GPi*
Gaussian	*STN-DBS*	198	102	132
Gaussian	*GPe-DBS*	186	76	108
Gaussian	*GPi-DBS*	188	74	124
Rectangular	*STN-DBS*	192	104	127
Rectangular	*GPe-DBS*	190	81	98
Rectangular	*GPi-DBS*	185	73	117

When it comes to measuring the synchronization of GPi neurons, Gaussian DBS was more promising in comparison with rectangular pulses, as can be seen in Figure 5.7. The SL (Equation 3.7) under healthy and PD conditions were 0.21 and 0.78, respectively. This higher synchronization due to PD was reported in [126]. The lowest SL was achieved by targeting GPi neurons with Gaussian signals. Gaussian DBS signals targeted at any location within the basal ganglia achieved lower SL compared to rectangular DBS signals. This states that Gaussian DBS waveforms are as efficient as rectangular pulses in terms of desynchronization of GPi neurons. The EC was measured by Equation 3.8 in the basal ganglia model with Gaussian and rectangular DBS signals targeted at different locations. As shown in Figure 5.7, Gaussian signals were able to activate the basal ganglia neurons with less amount of energy compared to rectangular DBS signals. Gaussian signals for DBS guarantee the minimum EC compared to any other signal form such as pulse, rectangular, ramp, exponential and sinusoid [14]. The lower EC would help PD patients to avoid a costly battery replacement surgery which is a critical challenge in DBS technology.
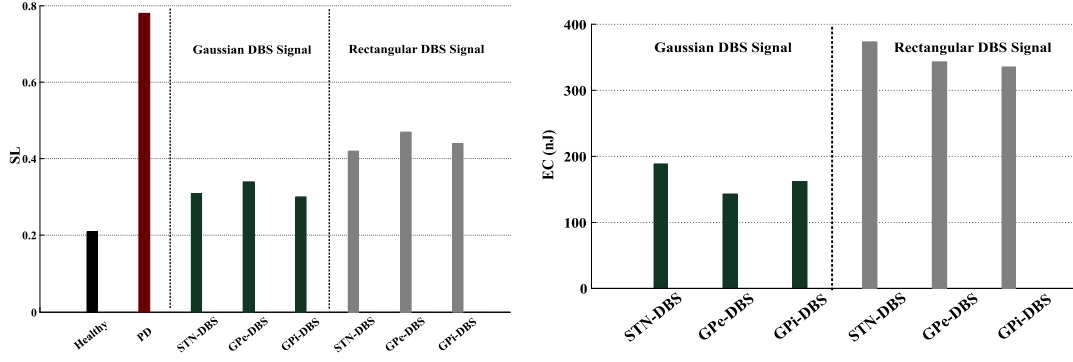
Figure 5.7 SL and EC computation for various DBS waveforms and targets

5.4   FAS Method Outcomes

In order to compare the effectiveness of FAS method we investigated some well-studied protocol such as Pulsatile delayed feedback [18], High Frequency Stimulation (HFS) [20, 102]and Variant Frequency stimulations (VFS) [27]. Similar to FAS the Pulsatile method uses the non-linearly delayed LFP signal as the control variable, however this control signal is used to modulate the amplitude of the DBS signal rather than its frequency [18]. HFS and VFS protocols on the other hand work in an open loop manner where the stimulation signal is pre-defined. The traditional HFS delivers high frequency pulses (> 130 Hz) for the duration of stimulation therapy [26, 105], while in the VFS protocol, fixed period blocks of high and low frequency stimulations are delivered according to a preset combinations such as HFS-LFS-LFS-LFS-HFS [27].

STN neurons had spontaneous firings at frequencies of 6 Hz and 8 Hz under healthy and PD conditions, respectively (Figure 5.8A, B). Although the healthy firing patterns matches the low firing rate characteristic of the STN cells observed in [127], the STN firings frequency under PD state was lower than actual recordings (30 Hz) [128] since certain connections in our model were strengthened. Under healthy condition, both GPe

55

and GPi neurons fire repetitive spikes, however in the PD state, the firing patterns changes to tonic bursts [3, 129]. According to [128] and Figure 5.8C, the firing rate of the STN neurons slightly increases from healthy to PD states.
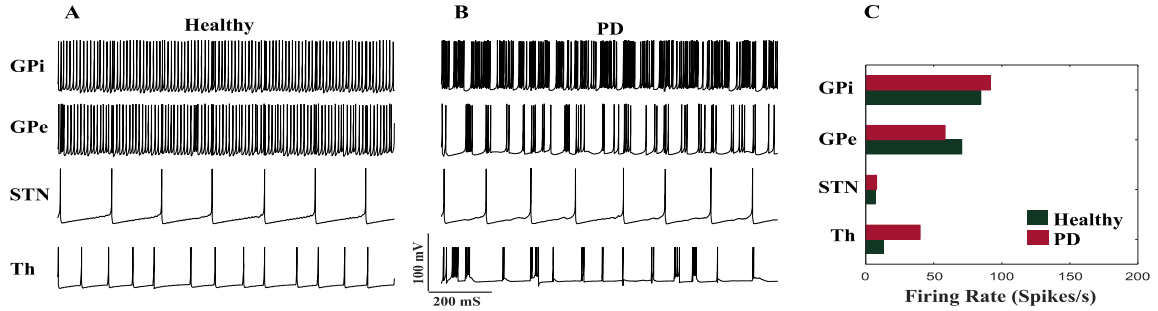
Figure 5.8 BG model neuronal firings and validation

In order to validate the dynamics of our BG model, we compared the average firing rates of STN, GPe and GPi neurons with the experimental recordings of normal (healthy) and MPTP-treated monkeys [122]. The results are shown in Table 5.2 and the firing rates (Spikes/s) are measured for both healthy and PD conditions [130]. As shown in Table 5.2, STN neurons fired more under PD conditions which is consistent with the experimental data and previous BG models [3, 122]. Similar to the recordings of MPTP-treated monkeys the firing rates of GPe neurons decreases under PD condition while GPi firing increases. All neuron types showed increased oscillatory behavior from healthy to PD conditions in the dominant frequency range of 8-15 Hz consistent with the experimental recordings [122].

Table 5.2 Characteristics of Neuronal Firings

		Proposed Method		Experimental Recordings [122]	
		Healthy	*PD*	*Healthy*	*MPTP*
Spikes/S	STN	12.5	16.7	23.2	37.3
	GPe	69.2	58.4	66.1	48.5
	GPi	76.8	85.6	73.5	78.1
Percentage of neurons oscillating between 8-15 Hz	STN	0.16%	63.20%	0%	50%
	GPe	12%	28%	9.10%	27.50%
Percentage of neurons oscillating higher than 15 Hz	STN	0.80%	11.2	0%	7.10%
	GPe	3.20%	4.80%	0%	2.50%
	GPi	5.60%	4%	3%	2.90%
Percentage of bursting neurons with 8-15 Hz oscillations	STN	0%	9.6%	0%	21.4%
	GPe	44%	26.4%	50%	0%
	GPi	8%	53.6%	0%	52.9%

The LFP is measured from a population of 125 STN neurons placed in a cubic area with 5 mm edges, according to Equation 3.18. The LFP signal is then filtered by the damped harmonic oscillator mentioned in Equation 3.19, to obtain $\dot{x}$. Figure 5.9 shows the original LFP with its filtered signal where the rhythmic behavior of the STN population is observable.
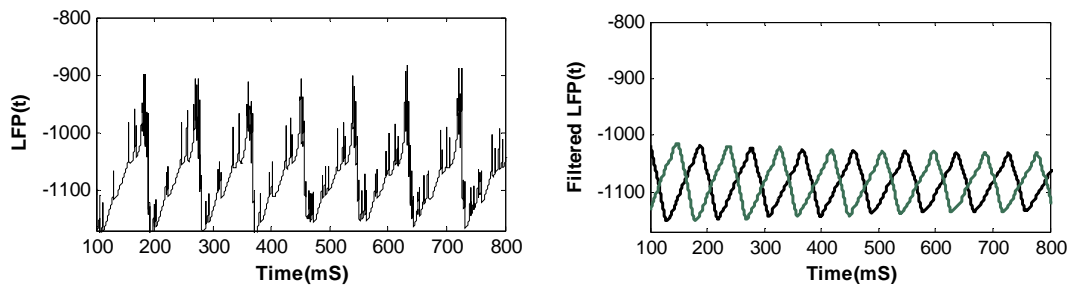
Figure 5.9 LFP and its filtered and delayed results

The LFP is measured from a population of 125 STN neurons placed in a cubic area with 5 mm edges, according to Equation 3.18. The LFP signal is then filtered by the damped harmonic oscillator mentioned in Equation 3.19, to obtain $\dot{x}$. Figure 5.9 shows the

original LFP with its filtered signal where the rhythmic behavior of the STN population is observable.

The FAS protocol incorporates the frequency modulation of I_{DBS} according to the amplitude of the feedback signal, as illustrated in Figure 5.10. The adjustment of the stimulation signal I_{DBS} according to the amplitude of the feedback signal is done via Equation 3.20. For high amplitudes of the feedback signal, an HFS stimulation signal (130Hz) is applied and as the amplitude descends, the frequency of stimulation shifts proportionally to lower frequencies until it eventually reaches a LFS (40Hz) stimulation signal. In order to avoid an irreversible charge deposit and tissue damage [101, 102], each period of stimulation signal concludes cathodic and anodic phases with a delay in between [10, 18, 127], as illustrated in Figure 3.3. This adjustment of I_{DBS} provides a charge balanced stimulus, impeding nervous tissue damages. The length of the cathodic, delay and anodic phases for the stimulus signal were set to 0.2, 0.5 and 2 *mS*, respectively, to guarantee a total charge close to zero for the biphasic stimulus pulse.
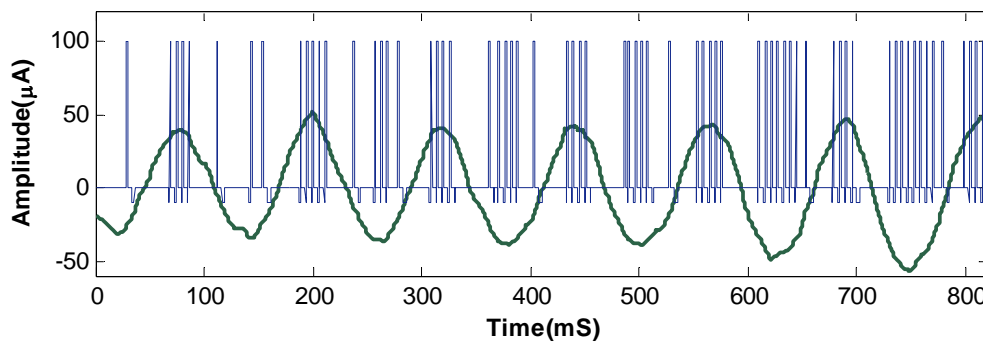
Figure 5.10 Adjusted stimulation signal by FAS protocol.

The Power Spectral Density (PSD) of the filtered LFP signal under healthy and PD states are depicted in Figure 5.11.
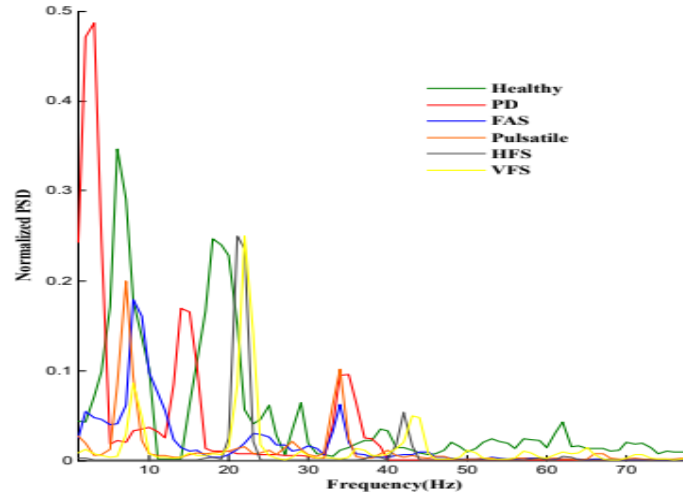
Figure 5.11 The normalized PSD of the LFP measurements for healthy, PD and different stimulation methods

Under healthy condition, the highest power occurred at 8 Hz and other peaks of the PSD were due to subsequent harmonics of the LFP signal. Our model was able to show a broad PSD peak at lower beta band at 14 Hz. This high power spectrum reflects the synchronous dynamics of the STN neuronal population firings. The STN population resonating with the GPe neurons causes the appearance of 34 Hz oscillation in PD. Both FAS and Pulsatile were able to suppress these oscillations, however, the 34 Hz oscillation was more suppressed by FAS compared to the Pulsatile protocol. Also, the first peak in the PSD of the FAS and pulsatile methods falls within the first peak of healthy PSD. FAS beta band oscillations were similar to [131] where irregular or adaptive frequency stimulation are shown to suppress the high beta band oscillations better than HFS or other closed-loop stimulation methods. On the other hand, HFS method shows to suppress the 14Hz oscillation, however from its PSD, we can see it does not match the healthy conditions oscillations. The PSD of HFS shows a main peak of oscillation at 23 Hz and a smaller oscillations at 43 Hz. The dynamics of PD in our model are shown through the spectrogram and raster plots of 125 STN neurons (Figure 5.12). We can observe a high synchronization

at low frequencies in the spectrogram of PD which is a significant property of pathological networks [129].
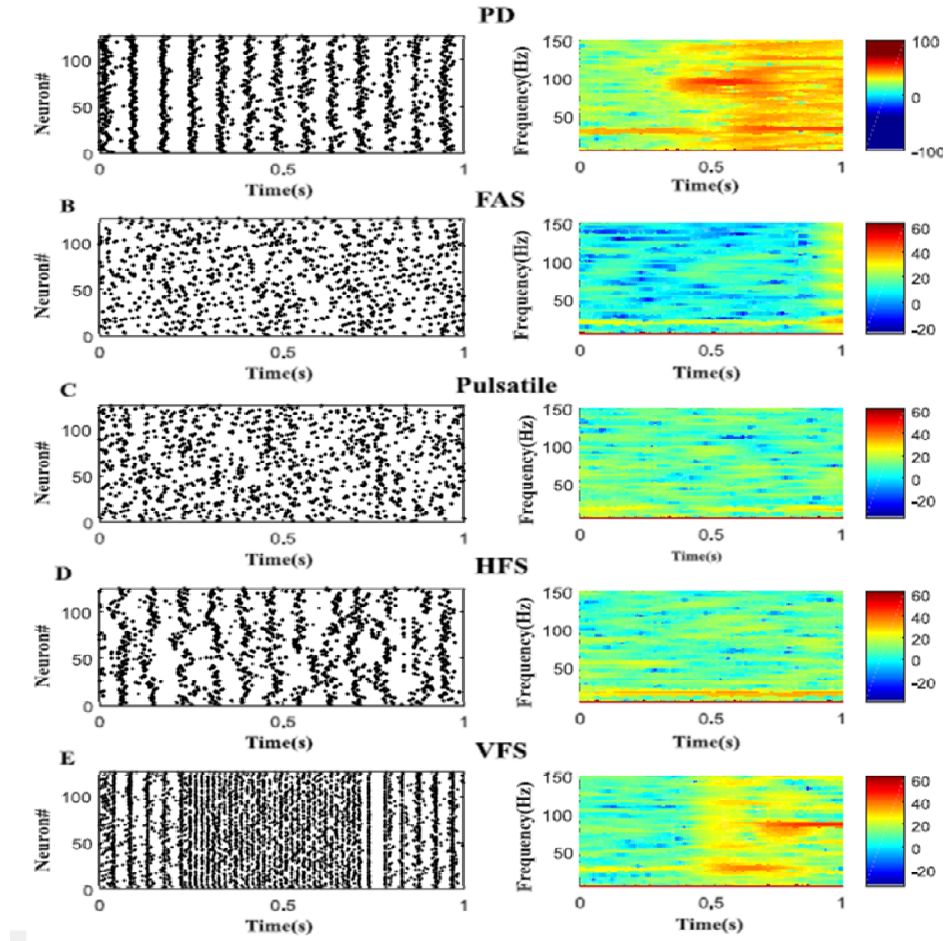
Figure 5.12 Raster plot and Spectrogram comparison of various open loop and closed loop stimulation protocols

Applying the DBS currents shows desynchronizing effects particularly at the low frequencies, as shown via the spectrograms of Figure 5.12. Comparing the spectrograms of 4 different stimulation protocols, we conclude that all stimulations were able to desynchronize the network at low frequencies, however closed loop FAS and Pulsatile methods were more effective. It was also observed that the power densities depicted by the spectrograms were more spread, which is consistent with patterns seen in patients

undergoing L-Dopa treatments [132]. According to the power density scale shown in the color bars of Figure 5.12, the FAS protocol achieves the highest desynchronization of the STN population.

5.5 Neuronavigation TMS Pipeline Results

As explained in section 3.6, the pipeline for the proposed neuronavigatin system has multiple modules, each requiring a specific software. Here, we present the results of each module based on Figure 3.5. The MRI data used in this study was obtained from the SimNIBS example files [75] as shown in Figure 2.8. The segmentation results for 1 slice of a T1 weighted MR image is shown in Figure 5.13.
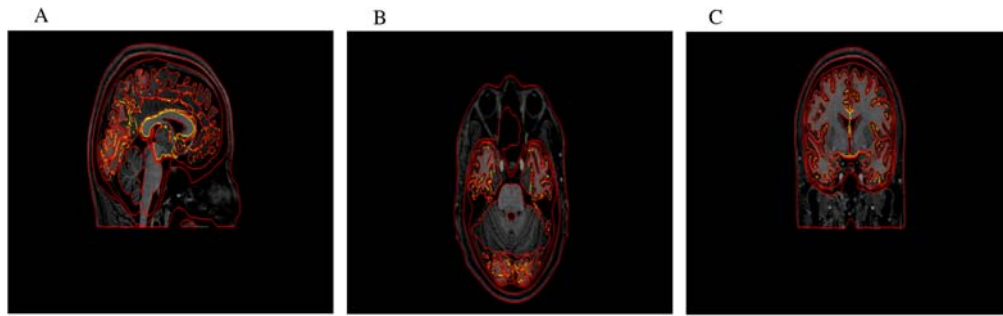
Figure 5.13 MRI tissue segmentaion

After decoupling the segmented areas and generating the surface and volume meshes, the surface mesh qualities are evaluated by 2 metrics of SICN and Gamma as shown in Figure 5.14. If the quality of the generated surface meshes was not satisfying, we run MeshFix to improve the quality [115].

Number of Triangles: 289146
SICN: 0.941
Gamma: 0.94

White Matter (VM)

Number of Triangles: 275266
SICN: 0.946
Gamma: 0.938

Grey Matter (GM)

Number of Triangles: 177562
SICN: 0.948
Gamma: 0.939

Skull

Number of Triangles: 89812
SICN: 0.948
Gamma: 0.938

Cerebrospinal Fluid (CSF)

Number of Triangles: 12430
SICN: 0.951
Gamma: 0.943

Cavities

Number of Triangles: 189385
SICN: 0.947
Gamma: 0.938

Skin
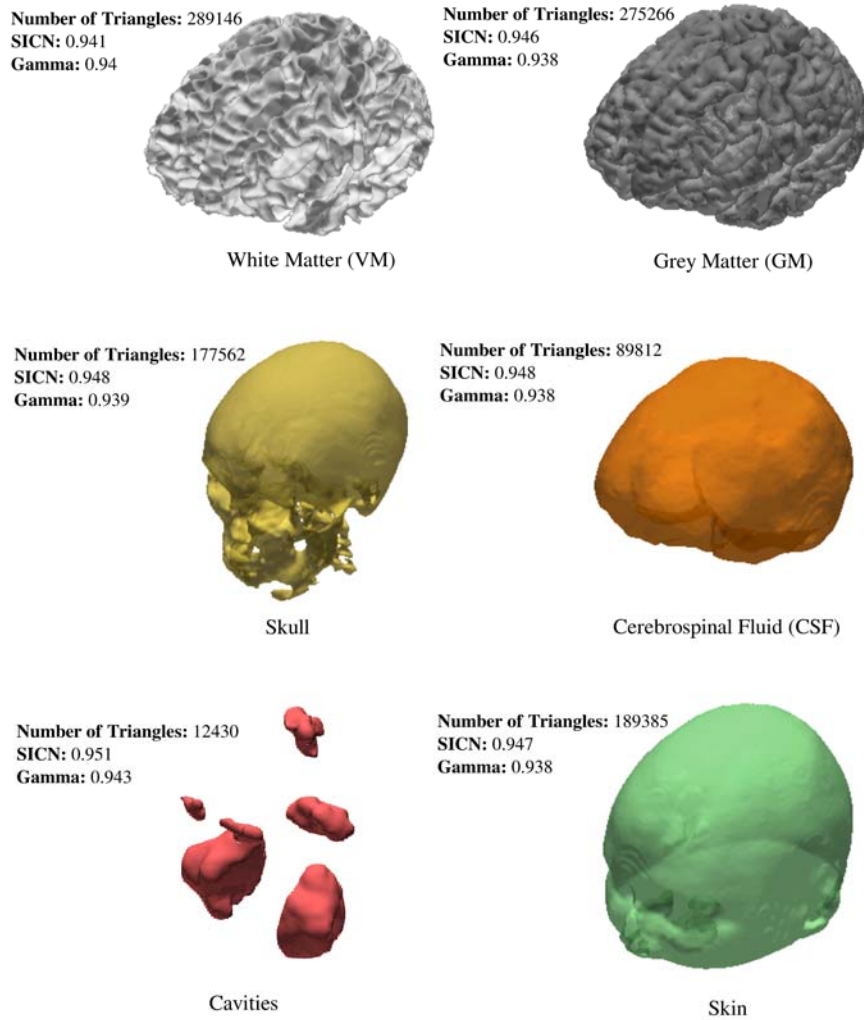
Figure 5.14 3D Volume meshes of segmented areas of MR images.

Once we obtain the desired 3D volume meshes (Figure 5.14), we need to validate to see if these volumes are reasonably registered with the MR images. For this, we manually define some point markers on the MR T1 weighted images and measure the distance of these points to the actual surface. In Figure 5.15 we can see that marker points

are relatively aligned with the 3D model of the skull and the average distance measured by Equation 3.22 was 1.37 voxel.

Figure 5.15 Model Validation with marker point trackers.

Furthermore, we measured the distance of marker points to VM, GM, CSF, Skin and Skull as shown in Table 5.3. For each volume type, we manually selected 20 marker points and measured the distance to the closest point on the surface. The low distance results on this table show a reasonable 3D volume extraction method from the MR images as explained in section 3.6.

Table 5.3 Distance Measure of Manually Selected Marker Points to the Various Brain Volumes.

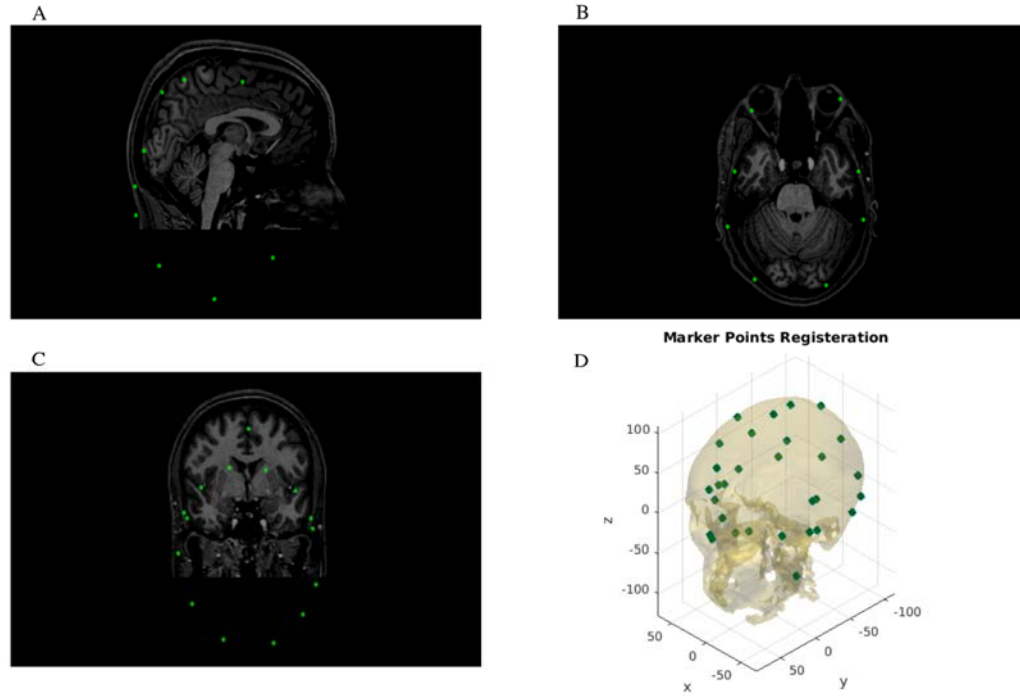| Marker Point	WM	GM	CSF	Skull	Skin
1	0.854	2.12	1.707	-0.043	-0.513
2	1.401	1.850	-0.512	0.536	-0.489
3	-3.055	2.661	-2.922	0.332	0.771
4	4.089	3.011	1.064	4.732	0.698
5	3.119	-0.907	1.089	0.904	1.833
6	2.648	-2.585	1.349	0.331	1.826
7	-0.372	-1.114	-0.057	3.565	1.679
8	-1.277	0.540	-0.859	-0.339	1.560
9	1.266	1.847	-0.574	-1.204	2.452
10	1.598	1.432	1.126	-2.0816	1.333
11	2.504	2.679	1.089	-0.842	-0.749
12	1.488	0.719	0.897	2.915	1.894
13	3.918	0.214	0.559	0.947	-1.263
14	0.079	1.617	-2.044	-1.079	0.251
15	-2.842	-2.050	0.054	-0.628	0.450
16	-3.713	0.338	0.198	1.677	-1.234
17	-1.094	-0.258	1.811	1.036	-0.818
18	0.922	-1.148	1.912	1.488	1.026
19	1.638	0.836	1.065	2.148	0.904
20	-2.217	0.469	0.736	-0.584	1.007
Average Distance	**2.004**	**1.419**	**1.082**	**1.371**	**1.137**

After the validation step, we need to adjust the voxel based coordinates to continuous coordinates, as described in equation 3.23. We used Freesurfer software for this transformation due to its robust method and clear visualization [74]. The obtained brain volumes with proper coordinates were then used to calculate the TMS Magnetic fields. We assumed a circular TMS coil placed over a specific location based on the EEG cortical map. The coil was placed at 4 mm distance from the surface of the head. The results were generated with MATLAB and SimNIBS software, as shown in Figure 5.16. In this figure, we showed the generated electrical fields due to the induced TMS magnetic fields, when the TMS coil is placed over AF4, C3, CP6 and Pz from the EEG cortical map.
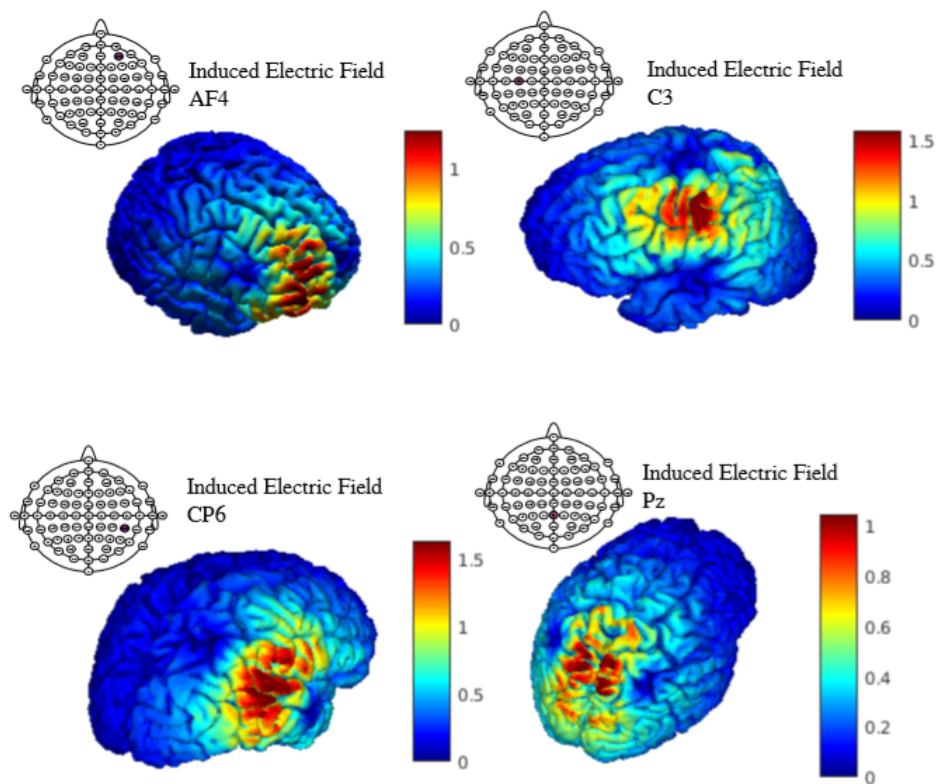
Figure 5.16 Electric fields induced by the TMS coil on the GM surface.

CHAPTER 6: CONCLUSION AND FUTURE DIRECTIONS

In neurodegenerative disorders such as PD, deep brain stimulation (DBS) is a desirable approach when the medication is less effective for treating the symptoms. DBS incorporates transferring electrical pulses to a specific tissue of the central nervous system, obtaining therapeutic results by modulating the neuronal activity of that region.

In this research, we presented a mathematical model to generate various neuronal spiking patterns. The key advantage of this hyperbolic model is the fact that it has low computational complexity and can produce various neuronal firing patters by only adjusting very few parameters. Additionally, we showed how modification of DBS waveforms in the network of the basal ganglia can be beneficial in comparison with standard rectangular DBS used in surgeries. Moreover, we implemented novel Gaussian signals with interphase delays on a more complex network of the basal ganglia, considering the interactions between various cell types. With Gaussian pulses for stimulation, we were able to reduce the delay period, which is safe to be used without causing tissue damage. In terms of energy consumption of DBS waveforms, we showed that placing the delay between two parts of the pulse balanced signal would significantly decrease the energy consumption and therefore provides a longer life time of Implantable Pulse Generator (IPG), avoiding costly replacement surgeries.

We also developed a 3-D computational model of four nuclei within the basal ganglia according to the reduced order model of Izhikevich. We significantly reduced the computational cost, while reliably capturing the neural activations and LFPs. The lower

computational cost provided the opportunity to investigate the effect of DBS on large-scale networks. Our model was able to generate the beta-band oscillations at 34 Hz with the burst firings of the STN neurons under PD or dopamine depletion. The FAS protocol in this research was incorporated in a delayed feedback closed loop manner. Adapted signals in a delayed feedback method can reduce the side effect of tissue damage, enhance the desynchronization performance and increase the battery life. Furthermore, as the beta-band oscillation does not appear consistently, closed loop stimulation of the beta-band with more pulses at higher synchronization and less at lower synchronization is more efficient than the traditional open loop stimulations. The FAS protocol has shown to be more efficient in the suppression of the STN oscillations along with generating a mixture of firing responses, which has been associated with the efficiency of DBS.

Finally, we proposed a neuronavigation system for TMS therapy which allows fast and robust stimulation of brain regions based on EEG cortical map. At the moment, this system is only available for single coil stimulation, however we aim to develop a multi coil neuronavigation system to improve the quality of stimulation [133]. The ultimate goal is to develop a new pipeline for fast and real-time multi-channel TMS stimulation.

REFERENCES

[1]   A. L. Hodgkin and A. F. Huxley, "A quantitative description of membrane current and its application to conduction and excitation in nerve," *The Journal of physiology,* vol. 117, no. 4, pp. 500-544, 1952.

[2]   E. M. Izhikevich, "Which model to use for cortical spiking neurons?," *IEEE transactions on neural networks,* vol. 15, no. 5, pp. 1063-1070, 2004.

[3]   R. Q. So, A. R. Kent, and W. M. Grill, "Relative contributions of local cell and passing fiber activation and silencing to changes in thalamic fidelity during deep brain stimulation and lesioning: a computational modeling study," *Journal of computational neuroscience,* vol. 32, no. 3, pp. 499-519, 2012.

[4]   S. Ratnadurai-Giridharan, C. C. Cheung, and L. L. Rubchinsky, "Effects of electrical and optogenetic deep brain stimulation on synchronized oscillatory activity in parkinsonian basal ganglia," *IEEE Transactions on Neural Systems and Rehabilitation Engineering,* vol. 25, no. 11, pp. 2188-2195, 2017.

[5]   C. Halpern, H. Hurtig, J. Jaggi, M. Grossman, M. Won, and G. Baltuch, "Deep brain stimulation in neurologic disorders," *Parkinsonism & related disorders,* vol. 13, no. 1, pp. 1-16, 2007.

[6]   A. M. Lozano, J. Dostrovsky, R. Chen, and P. Ashby, "Deep brain stimulation for Parkinson's disease: disrupting the disruption," *The Lancet Neurology,* vol. 1, no. 4, pp. 225-231, 2002.

[7] B. Wingeier, T. Tcheng, M. M. Koop, B. C. Hill, G. Heit, and H. M. Bronte-Stewart, "Intra-operative STN DBS attenuates the prominent beta rhythm in the STN in Parkinson's disease," *Experimental neurology,* vol. 197, no. 1, pp. 244-251, 2006.

[8] N. Maling, R. Hashemiyoon, K. D. Foote, M. S. Okun, and J. C. Sanchez, "Increased thalamic gamma band activity correlates with symptom relief following deep brain stimulation in humans with Tourette's syndrome," *PloS one,* vol. 7, no. 9, p. e44215, 2012.

[9] M. Daneshzand, M. Faezipour, and B. D. Barkana, "Computational Stimulation of the Basal Ganglia Neurons with Cost Effective Delayed Gaussian Waveforms," *Frontiers in computational neuroscience,* vol. 11, p. 73, 2017.

[10] S. Miocinovic *et al.*, "Computational analysis of subthalamic nucleus and lenticular fasciculus activation during therapeutic deep brain stimulation," *Journal of neurophysiology,* vol. 96, no. 3, pp. 1569-1580, 2006.

[11] M. Pirini, L. Rocchi, M. Sensi, and L. Chiari, "A computational modelling approach to investigate different targets in deep brain stimulation for Parkinson's disease," *Journal of computational neuroscience,* vol. 26, no. 1, p. 91, 2009.

[12] T. J. Foutz and C. C. McIntyre, "Evaluation of novel stimulus waveforms for deep brain stimulation," *Journal of neural engineering,* vol. 7, no. 6, p. 066008, 2010.

[13] A. B. Holt, D. Wilson, M. Shinn, J. Moehlis, and T. I. Netoff, "Phasic burst stimulation: a closed-loop approach to tuning deep brain stimulation parameters for parkinson's disease," *PLoS computational biology,* vol. 12, no. 7, p. e1005011, 2016.

[14] A. Wongsarnpigoon and W. M. Grill, "Energy-efficient waveform shapes for neural stimulation revealed with a genetic algorithm," *Journal of neural engineering,* vol. 7, no. 4, p. 046009, 2010.

[15] L. Hofmann, M. Ebert, P. A. Tass, and C. Hauptmann, "Modified pulse shapes for effective neural stimulation," *Frontiers in neuroengineering,* vol. 4, p. 9, 2011.

[16] P. F. Grant and M. M. Lowery, "Simulation of cortico-basal ganglia oscillations and their suppression by closed loop deep brain stimulation," *IEEE Transactions on neural systems and rehabilitation engineering,* vol. 21, no. 4, pp. 584-594, 2013.

[17] M. Daneshzand, S. A. Ibrahim, M. Faezipour, and B. D. Barkana, "Desynchronization and Energy Efficiency of Gaussian Neurostimulation on Different Sites of the Basal Ganglia," in *Bioinformatics and Bioengineering (BIBE), 2017 IEEE 17th International Conference on*, 2017, pp. 57-62: IEEE.

[18] O. V. Popovych, B. Lysyansky, and P. A. Tass, "Closed-loop deep brain stimulation by pulsatile delayed feedback with increased gap between pulse phases," *Scientific reports,* vol. 7, no. 1, p. 1033, 2017.

[19] A. M. Kuncel and W. M. Grill, "Selection of stimulus parameters for deep brain stimulation," *Clinical neurophysiology,* vol. 115, no. 11, pp. 2431-2441, 2004.

[20] L. Garcia, G. D'Alessandro, B. Bioulac, and C. Hammond, "High-frequency stimulation in Parkinson's disease: more or less?," *Trends in neurosciences,* vol. 28, no. 4, pp. 209-216, 2005.

[21] T. Hashimoto, C. M. Elder, M. S. Okun, S. K. Patrick, and J. L. Vitek, "Stimulation of the subthalamic nucleus changes the firing pattern of pallidal neurons," *Journal of neuroscience,* vol. 23, no. 5, pp. 1916-1923, 2003.

[22]   S. R. Summerson, B. Aazhang, and C. Kemere, "Investigating irregularly patterned deep brain stimulation signal design using biophysical models," *Frontiers in computational neuroscience,* vol. 9, p. 78, 2015.

[23]   J. E. Rubin and D. Terman, "High frequency stimulation of the subthalamic nucleus eliminates pathological thalamic rhythmicity in a computational model," *Journal of computational neuroscience,* vol. 16, no. 3, pp. 211-235, 2004.

[24]   A. Vakil, H. Homayoun, and A. Sasan, "IR-ATA: IR annotated timing analysis, a flow for closing the loop between PDN design, IR analysis & timing closure," in *Proceedings of the 24th Asia and South Pacific Design Automation Conference*, 2019, pp. 152-159: ACM.

[25]   M. Daneshzand, M. Faezipour, and B. D. Barkana, "Towards frequency adaptation for delayed feedback deep brain stimulations," *Neural regeneration research,* vol. 13, no. 3, p. 408, 2018.

[26]   M.-L. Welter *et al.*, "Effects of high-frequency stimulation on subthalamic neuronal activity in parkinsonian patients," *Archives of neurology,* vol. 61, no. 1, pp. 89-96, 2004.

[27]   F. Jia *et al.*, "Variable frequency stimulation of subthalamic nucleus in Parkinson's disease: Rationale and hypothesis," *Parkinsonism & related disorders,* vol. 39, pp. 27-30, 2017.

[28]   F. Windels, N. Bruet, A. Poupard, C. Feuerstein, A. Bertrand, and M. Savasta, "Influence of the frequency parameter on extracellular glutamate and γ aminobutyric acid in substantia nigra and globus pallidus during electrical

stimulation of subthalamic nucleus in rats," *Journal of neuroscience research,* vol. 72, no. 2, pp. 259-267, 2003.

[29] J. M. Deniau, B. Degos, C. Bosch, and N. Maurice, "Deep brain stimulation mechanisms: beyond the concept of local functional inhibition," *European Journal of Neuroscience,* vol. 32, no. 7, pp. 1080-1091, 2010.

[30] R. S. George, J. Nutt, K. Burchiel, and F. Horak, "A meta-regression of the long-term effects of deep brain stimulation on balance and gait in PD," *Neurology,* vol. 75, no. 14, pp. 1292-1299, 2010.

[31] J. Modolo, J. Henry, and A. Beuter, "Dynamics of the subthalamo-pallidal complex in Parkinson's disease during deep brain stimulation," *Journal of biological physics,* vol. 34, no. 3-4, pp. 251-266, 2008.

[32] P. A. Tass, "A model of desynchronizing deep brain stimulation with a demand-controlled coordinated reset of neural subpopulations," *Biological cybernetics,* vol. 89, no. 2, pp. 81-88, 2003.

[33] A. D. Dorval, A. M. Kuncel, M. J. Birdno, D. A. Turner, and W. M. Grill, "Deep brain stimulation alleviates parkinsonian bradykinesia by regularizing pallidal activity," *Journal of neurophysiology,* vol. 104, no. 2, pp. 911-921, 2010.

[34] M. D. Humphries and K. Gurney, "Network effects of subthalamic deep brain stimulation drive a unique mixture of responses in basal ganglia output," *European journal of neuroscience,* vol. 36, no. 2, pp. 2240-2251, 2012.

[35] G. C. McConnell, R. Q. So, J. D. Hilliard, P. Lopomo, and W. M. Grill, "Effective deep brain stimulation suppresses low-frequency network oscillations in the basal

ganglia by regularizing neural firing patterns," *Journal of Neuroscience,* vol. 32, no. 45, pp. 15657-15668, 2012.

[36]   J. C. Lilly, J. R. Hughes, E. C. Alvord Jr, and T. W. Galkin, "Brief, noninjurious electric waveform for stimulation of the brain," *Science,* 1955.

[37]   M. Sahin and Y. Tie, "Non-rectangular waveforms for neural stimulation with practical electrodes," *Journal of neural engineering,* vol. 4, no. 3, p. 227, 2007.

[38]   S. Jezernik and M. Morari, "Energy-optimal electrical excitation of nerve fibers," *IEEE Transactions on Biomedical Engineering,* vol. 52, no. 4, pp. 740-743, 2005.

[39]   R. J. Coffey, "Deep brain stimulation devices: a brief technical history and review," *Artificial organs,* vol. 33, no. 3, pp. 208-220, 2009.

[40]   E. Moro, R. Esselink, J. Xie, M. Hommel, A. Benabid, and P. Pollak, "The impact on Parkinson's disease of electrical parameter settings in STN stimulation," *Neurology,* vol. 59, no. 5, pp. 706-713, 2002.

[41]   A. Dovzhenok, C. Park, R. M. Worth, and L. L. Rubchinsky, "Failure of delayed feedback deep brain stimulation for intermittent pathological synchronization in Parkinson's disease," *PLoS One,* vol. 8, no. 3, p. e58264, 2013.

[42]   K. Gurney, T. J. Prescott, and P. Redgrave, "A computational model of action selection in the basal ganglia. I. A new functional anatomy," *Biological cybernetics,* vol. 84, no. 6, pp. 401-410, 2001.

[43]   E. M. Izhikevich, *Dynamical systems in neuroscience*. MIT press, 2007.

[44]   K. Gunalan, B. Howell, and C. C. McIntyre, "Quantifying axonal responses in patient-specific models of subthalamic deep brain stimulation," *Neuroimage,* vol. 172, pp. 263-277, 2018.

[45]   B. D. Greenberg *et al.*, "Three-year outcomes in deep brain stimulation for highly resistant obsessive–compulsive disorder," *Neuropsychopharmacology,* vol. 31, no. 11, p. 2384, 2006.

[46]   K. Østergaard and N. Aa. Sunde, "Evolution of Parkinson's disease during 4 years of bilateral deep brain stimulation of the subthalamic nucleus," *Movement disorders: official journal of the Movement Disorder Society,* vol. 21, no. 5, pp. 624-631, 2006.

[47]   A.-L. Benabid, P. Krack, A. Benazzouz, P. Limousin, A. Koudsie, and P. Pollak, "Deep brain stimulation of the subthalamic nucleus for Parkinson's disease: methodologic aspects and clinical criteria," *Neurology,* vol. 55, no. 12 Suppl 6, pp. S40-4, 2000.

[48]   M. Rodriguez-Oroz *et al.*, "Bilateral deep brain stimulation in Parkinson's disease: a multicentre study with 4 years follow-up," *Brain,* vol. 128, no. 10, pp. 2240-2249, 2005.

[49]   M. E. Anderson, N. Postupna, and M. Ruffo, "Effects of high-frequency stimulation in the internal globus pallidus on the activity of thalamic neurons in the awake monkey," *Journal of neurophysiology,* vol. 89, no. 2, pp. 1150-1160, 2003.

[50]   S. Little *et al.*, "Adaptive deep brain stimulation in advanced Parkinson disease," *Annals of neurology,* vol. 74, no. 3, pp. 449-457, 2013.

[51]   A. Vakil and H. Bajwa, "Energy harvesting using Graphene based antenna for UV spectrum," in *IEEE Long Island Systems, Applications and Technology (LISAT) Conference 2014*, 2014, pp. 1-4: IEEE.

[52] A. Berney *et al.*, "Effect on mood of subthalamic DBS for Parkinson's disease A consecutive series of 24 patients," *Neurology,* vol. 59, no. 9, pp. 1427-1429, 2002.

[53] M. Rizzone *et al.*, "Long-term outcome of subthalamic nucleus DBS in Parkinson's disease: from the advanced phase towards the late stage of the disease?," *Parkinsonism & related disorders,* vol. 20, no. 4, pp. 376-381, 2014.

[54] J. L. Abelson *et al.*, "Deep brain stimulation for refractory obsessive-compulsive disorder," *Biological psychiatry,* vol. 57, no. 5, pp. 510-516, 2005.

[55] G. I. Detorakis, A. Chaillet, S. Palfi, and S. Senova, "Closed-loop stimulation of a delayed neural fields model of parkinsonian STN-GPe network: a theoretical and computational study," *Frontiers in neuroscience,* vol. 9, p. 237, 2015.

[56] S. F. Cogan, K. A. Ludwig, C. G. Welle, and P. Takmakov, "Tissue damage thresholds during therapeutic electrical stimulation," *Journal of neural engineering,* vol. 13, no. 2, p. 021001, 2016.

[57] D. J. DiLorenzo, J. Jankovic, R. K. Simpson, H. Takei, and S. Z. Powell, "Neurohistopathological findings at the electrode–tissue interface in long term deep brain stimulation: systematic literature review, case report, and assessment of stimulation threshold safety," *Neuromodulation: Technology at the Neural Interface,* vol. 17, no. 5, pp. 405-418, 2014.

[58] D. Harnack, C. Winter, W. Meissner, T. Reum, A. Kupsch, and R. Morgenstern, "The effects of electrode material, charge density and stimulation duration on the safety of high-frequency stimulation of the subthalamic nucleus in rats," *Journal of neuroscience methods,* vol. 138, no. 1-2, pp. 207-216, 2004.

[59] B. Rosin *et al.*, "Closed-loop deep brain stimulation is superior in ameliorating parkinsonism," *Neuron,* vol. 72, no. 2, pp. 370-384, 2011.

[60] K. E. Lyons, S. B. Wilkinson, J. Overman, and R. Pahwa, "Surgical and hardware complications of subthalamic stimulation A series of 160 procedures," *Neurology,* vol. 63, no. 4, pp. 612-616, 2004.

[61] J. Bolam, J. Hanley, P. Booth, and M. Bevan, "Synaptic organisation of the basal ganglia," *The Journal of Anatomy,* vol. 196, no. 4, pp. 527-542, 2000.

[62] A. B. Holt and T. I. Netoff, "Origins and suppression of oscillations in a computational model of Parkinson's disease," *Journal of computational neuroscience,* vol. 37, no. 3, pp. 505-521, 2014.

[63] A. Priori, G. Foffani, L. Rossi, and S. Marceglia, "Adaptive deep brain stimulation (aDBS) controlled by local field potential oscillations," *Experimental neurology,* vol. 245, pp. 77-86, 2013.

[64] A. Riehle, S. Wirtssohn, S. Grün, and T. Brochier, "Mapping the spatio-temporal structure of motor cortical LFP and spiking activities during reach-to-grasp movements," *Frontiers in neural circuits,* vol. 7, p. 48, 2013.

[65] O. V. Popovych, C. Hauptmann, and P. A. Tass, "Effective desynchronization by nonlinear delayed feedback," *Physical review letters,* vol. 94, no. 16, p. 164102, 2005.

[66] H. R. Siebner *et al.*, "Lasting cortical activation after repetitive TMS of the motor cortex A glucose metabolic study," *Neurology,* vol. 54, no. 4, pp. 956-963, 2000.

[67]   S. Pridmore, S. Erger, M. Rybak, E. Kelly, and T. May, "Early relapse (ER) transcranial magnetic stimulation (TMS) in treatment resistant major depression," *Brain stimulation,* 2018.

[68]   A. Mohammadi, "Implementation of a theoretical pipeline for modeling navigated transcranial magnetic stimulation," 2018.

[69]   A. T. Barker, R. Jalinous, and I. L. Freeston, "Non-invasive magnetic stimulation of human motor cortex," *The Lancet,* vol. 325, no. 8437, pp. 1106-1107, 1985.

[70]   A. Nummenmaa *et al.*, "Targeting of white matter tracts with transcranial magnetic stimulation," *Brain stimulation,* vol. 7, no. 1, pp. 80-84, 2014.

[71]   M. Windhoff, A. Opitz, and A. Thielscher, "Electric field calculations in brain stimulation based on finite elements: an optimized processing pipeline for the generation and usage of accurate individual head models," *Human brain mapping,* vol. 34, no. 4, pp. 923-935, 2013.

[72]   S. Makarov, G. Noetscher, T. Raij, and A. Nummenmaa, "A Quasi-Static Boundary Element Approach with Fast Multipole Acceleration for High-Resolution Bioelectromagnetic Models," *IEEE Transactions on Biomedical Engineering,* 2018.

[73]   J. Ruohonen and R. Ilmoniemi, "Focusing and targeting of magnetic brain stimulation using multiple coils," *Medical and Biological Engineering and Computing,* vol. 36, no. 3, pp. 297-301, 1998.

[74]   B. Fischl, "FreeSurfer," *Neuroimage,* vol. 62, no. 2, pp. 774-781, 2012.

[75]   G. Saturnino, A. Antunes, J. Stelzer, and A. Thielscher, "SimNIBS: A versatile toolbox for simulating fields generated by transcranial brain stimulation," in *21st*

Annual Meeting of the Organization for Human Brain Mapping (OHBM 2015), 2015.

[76] R. Goebel, F. Esposito, and E. Formisano, "Analysis of FIAC data with BrainVoyager QX: from single-subject to cortically aligned group GLM analysis and self-organizing group ICA," *Hum. Brain Mapp,* vol. 27, no. 5, pp. 392-401, 2006.

[77] R. Johnson and R. Stacey, "The impact of new imaging technologies in neurosurgery," *The Surgeon,* vol. 6, no. 6, pp. 344-349, 2008.

[78] M. Bikson, A. Rahman, and A. Datta, "Computational models of transcranial direct current stimulation," *Clinical EEG and Neuroscience,* vol. 43, no. 3, pp. 176-183, 2012.

[79] R. Mehrizi, X. Peng, Z. Tang, X. Xu, D. Metaxas, and K. Li, "Toward Marker-free 3D Pose Estimation in Lifting: A Deep Multi-view Solution," in *Automatic Face & Gesture Recognition (FG 2018), 2018 13th IEEE International Conference on*, 2018, pp. 485-491: IEEE.

[80] R. Mehrizi, X. Peng, X. Xu, S. Zhang, D. Metaxas, and K. Li, "A computer vision based method for 3D posture estimation of symmetrical lifting," *Journal of biomechanics,* vol. 69, pp. 40-46, 2018.

[81] M. Daneshzand, M. Faezipour, and B. D. Barkana, "Hyperbolic Modeling of Subthalamic Nucleus Cells to Investigate the Effect of Dopamine Depletion," *Computational intelligence and neuroscience,* vol. 2017, 2017.

[82] N. Ray *et al.*, "Local field potential beta activity in the subthalamic nucleus of patients with Parkinson's disease is associated with improvements in bradykinesia

after dopamine and deep brain stimulation," *Experimental neurology,* vol. 213, no. 1, pp. 108-113, 2008.

[83]   A. A. Kühn *et al.*, "Pathological synchronisation in the subthalamic nucleus of patients with Parkinson's disease relates to both bradykinesia and rigidity," *Experimental neurology,* vol. 215, no. 2, pp. 380-387, 2009.

[84]   W. Gerstner and R. Brette, "Adaptive exponential integrate-and-fire model," *Scholarpedia,* vol. 4, no. 6, p. 8427, 2009.

[85]   C. Beurrier, P. Congar, B. Bioulac, and C. Hammond, "Subthalamic nucleus neurons switch from single-spike activity to burst-firing mode," *Journal of Neuroscience,* vol. 19, no. 2, pp. 599-609, 1999.

[86]   C. C. McIntyre, M. Savasta, L. Kerkerian-Le Goff, and J. L. Vitek, "Uncovering the mechanism (s) of action of deep brain stimulation: activation, inhibition, or both," *Clinical neurophysiology,* vol. 115, no. 6, pp. 1239-1248, 2004.

[87]   L. S. Morris, K. Baek, and V. Voon, "Distinct cortico-striatal connections with subthalamic nucleus underlie facets of compulsivity," *cortex,* vol. 88, pp. 143-150, 2017.

[88]   F. Piedimonte *et al.*, "Behavioral and Motor Improvement After Deep Brain Stimulation of the Globus Pallidus Externus in a Case of T ourette's Syndrome," *Neuromodulation: Technology at the Neural Interface,* vol. 16, no. 1, pp. 55-58, 2013.

[89]   M. R. DeLong and T. Wichmann, "Circuits and circuit disorders of the basal ganglia," *Archives of neurology,* vol. 64, no. 1, pp. 20-24, 2007.

[90]   Y. Kuramoto, *Chemical oscillations, waves, and turbulence*. Springer Science & Business Media, 2012.

[91]   M. Daneshzand, M. Faezipour, and B. D. Barkana, "Robust desynchronization of Parkinson's disease pathological oscillations by frequency modulation of delayed feedback deep brain stimulation," *PloS one,* vol. 13, no. 11, p. e0207761, 2018.

[92]   A. Oswal *et al.*, "Deep brain stimulation modulates synchrony within spatially and spectrally distinct resting state networks in Parkinson's disease," *Brain,* vol. 139, no. 5, pp. 1482-1496, 2016.

[93]   A. G. Androulidakis *et al.*, "Amplitude modulation of oscillatory activity in the subthalamic nucleus during movement," *European Journal of Neuroscience,* vol. 27, no. 5, pp. 1277-1284, 2008.

[94]   M. Beudel and P. Brown, "Adaptive deep brain stimulation in Parkinson's disease," *Parkinsonism & related disorders,* vol. 22, pp. S123-S126, 2016.

[95]   A. A. Kühn and J. Volkmann, "Innovations in deep brain stimulation methodology," *Movement Disorders,* vol. 32, no. 1, pp. 11-19, 2017.

[96]   J. C. Lévesque and A. Parent, "GABAergic interneurons in human subthalamic nucleus," *Movement Disorders,* vol. 20, no. 5, pp. 574-584, 2005.

[97]   A. K. Engel and P. Fries, "Beta-band oscillations—signalling the status quo?," *Current opinion in neurobiology,* vol. 20, no. 2, pp. 156-165, 2010.

[98]   A. Moran and I. Bar-Gad, "Revealing neuronal functional organization through the relation between multi-scale oscillatory extracellular signals," *Journal of neuroscience methods,* vol. 186, no. 1, pp. 116-129, 2010.

[99] C. Eliasmith *et al.*, "A large-scale model of the functioning brain," *science,* vol. 338, no. 6111, pp. 1202-1205, 2012.

[100] M. D. Bevan and C. J. Wilson, "Mechanisms underlying spontaneous oscillation and rhythmic firing in rat subthalamic neurons," *Journal of Neuroscience,* vol. 19, no. 17, pp. 7617-7628, 1999.

[101] M. D. Johnson *et al.*, "Neuromodulation for brain disorders: challenges and opportunities," *IEEE Transactions on Biomedical Engineering,* vol. 60, no. 3, pp. 610-624, 2013.

[102] A. L. Jensen and D. M. Durand, "High frequency stimulation can block axonal conduction," *Experimental neurology,* vol. 220, no. 1, pp. 57-70, 2009.

[103] R. D. Traub and R. Miles, *Neuronal networks of the hippocampus*. Cambridge University Press, 1991.

[104] P. Brown, "Oscillatory nature of human basal ganglia activity: relationship to the pathophysiology of Parkinson's disease," *Movement Disorders,* vol. 18, no. 4, pp. 357-363, 2003.

[105] A. Stefani *et al.*, "Bilateral deep brain stimulation of the pedunculopontine and subthalamic nuclei in severe Parkinson's disease," *Brain,* vol. 130, no. 6, pp. 1596-1607, 2007.

[106] A. Nummenmaa, M. Stenroos, R. J. Ilmoniemi, Y. C. Okada, M. S. Hämäläinen, and T. Raij, "Comparison of spherical and realistically shaped boundary element head models for transcranial magnetic stimulation navigation," *Clinical Neurophysiology,* vol. 124, no. 10, pp. 1995-2007, 2013.

[107] M. Finke, T. Fadini, S. Kantelhardt, A. Giese, L. Matthaus, and A. Schweikard, "Brain-mapping using robotized TMS," in *Engineering in Medicine and Biology Society, 2008. EMBS 2008. 30th Annual International Conference of the IEEE*, 2008, pp. 3929-3932: IEEE.

[108] E. M. Wassermann, L. M. McShane, M. Hallett, and L. G. Cohen, "Noninvasive mapping of muscle representations in human motor cortex," *Electroencephalography and Clinical Neurophysiology/Evoked Potentials Section,* vol. 85, no. 1, pp. 1-8, 1992.

[109] Y. Huang, J. P. Dmochowski, Y. Su, A. Datta, C. Rorden, and L. C. Parra, "Automated MRI segmentation for individualized modeling of current flow in the human head," *Journal of neural engineering,* vol. 10, no. 6, p. 066004, 2013.

[110] A. Broumand, M. S. Esfahani, B.-J. Yoon, and E. R. Dougherty, "Discrete optimal Bayesian classification with error-conditioned sequential sampling," *Pattern Recognition,* vol. 48, no. 11, pp. 3766-3782, 2015.

[111] Q. Fang and D. A. Boas, "Tetrahedral mesh generation from volumetric binary and grayscale images," in *Biomedical Imaging: From Nano to Macro, 2009. ISBI'09. IEEE International Symposium on*, 2009, pp. 1142-1145: Ieee.

[112] D. A. Belsley, E. Kuh, and R. E. Welsch, *Regression diagnostics: Identifying influential data and sources of collinearity*. John Wiley & Sons, 2005.

[113] A. Broumand and T. Hu, "A length bias corrected likelihood ratio test for the detection of differentially expressed pathways in RNA-Seq data," in *Signal and Information Processing (GlobalSIP), 2015 IEEE Global Conference on*, 2015, pp. 1145-1149: IEEE.

[114] C. Geuzaine and J. F. Remacle, "Gmsh: A 3‑D finite element mesh generator with built‑in pre‑ and post‑processing facilities," *International journal for numerical methods in engineering,* vol. 79, no. 11, pp. 1309-1331, 2009.

[115] M. Attene, "A lightweight approach to repairing digitized polygon meshes," *The visual computer,* vol. 26, no. 11, pp. 1393-1406, 2010.

[116] B. Fischl, M. I. Sereno, and A. M. Dale, "Cortical surface-based analysis: II: inflation, flattening, and a surface-based coordinate system," *Neuroimage,* vol. 9, no. 2, pp. 195-207, 1999.

[117] P. Yu *et al.*, "Cortical surface shape analysis based on spherical wavelets," *IEEE transactions on medical imaging,* vol. 26, no. 4, pp. 582-597, 2007.

[118] C. J. Wilson and M. D. Bevan, "Intrinsic dynamics and synaptic inputs control the activity patterns of subthalamic nucleus neurons in health and in Parkinson's disease," *Neuroscience,* vol. 198, pp. 54-68, 2011.

[119] H. Bergman *et al.*, "Physiological aspects of information processing in the basal ganglia of normal and parkinsonian primates," *Trends in neurosciences,* vol. 21, no. 1, pp. 32-38, 1998.

[120] J. Baufreton and M. D. Bevan, "D2‑like dopamine receptor‑mediated modulation of activity‑dependent plasticity at GABAergic synapses in the subthalamic nucleus," *The Journal of physiology,* vol. 586, no. 8, pp. 2121-2142, 2008.

[121] T. Boraud, E. Bezard, D. Guehl, B. Bioulac, and C. Gross, "Effects of L-DOPA on neuronal activity of the globus pallidus externalis (GPe) and globus pallidus internalis (GPi) in the MPTP-treated monkey," *Brain research,* vol. 787, no. 1, pp. 157-160, 1998.

[122] T. Wichmann and J. Soares, "Neuronal firing before and after burst discharges in the monkey basal ganglia is predictably patterned in the normal state and altered in parkinsonism," *Journal of neurophysiology,* vol. 95, no. 4, pp. 2120-2133, 2006.

[123] J. Fell and N. Axmacher, "The role of phase synchronization in memory processes," *Nature reviews neuroscience,* vol. 12, no. 2, p. 105, 2011.

[124] M. Jalili, E. Barzegaran, and M. G. Knyazeva, "Synchronization of EEG: Bivariate and multivariate measures," *IEEE Trans. Neural Syst. Rehabil. Eng,* vol. 22, no. 2, pp. 212-221, 2014.

[125] J. L. Vitek, T. Hashimoto, J. Peoples, M. R. DeLong, and R. A. Bakay, "Acute stimulation in the external segment of the globus pallidus improves parkinsonian motor signs," *Movement disorders: official journal of the Movement Disorder Society,* vol. 19, no. 8, pp. 907-915, 2004.

[126] C. Hammond, H. Bergman, and P. Brown, "Pathological synchronization in Parkinson's disease: networks, models and treatments," *Trends in neurosciences,* vol. 30, no. 7, pp. 357-364, 2007.

[127] M. D. Bevan, P. J. Magill, D. Terman, J. P. Bolam, and C. J. Wilson, "Move to the rhythm: oscillations in the subthalamic nucleus–external globus pallidus network," *Trends in neurosciences,* vol. 25, no. 10, pp. 525-531, 2002.

[128] F. Steigerwald *et al.*, "Neuronal activity of the human subthalamic nucleus in the parkinsonian and nonparkinsonian state," *Journal of neurophysiology,* vol. 100, no. 5, pp. 2515-2524, 2008.

[129] A. Latteri, P. Arena, and P. Mazzone, "Characterizing Deep Brain Stimulation effects in computationally efficient neural network models," *Nonlinear biomedical physics,* vol. 5, no. 1, p. 2, 2011.

[130] M. Daneshzand, "Delayed Feedback Frequency Adjustment for Deep Brain Stimulation of Subthalamic Nucleus Oscillations," in *2018 40th Annual International Conference of the IEEE Engineering in Medicine and Biology Society (EMBC)*, 2018, pp. 2194-2197: IEEE.

[131] B.-P. Bejjani *et al.*, "Axial parkinsonian symptoms can be improved: the role of levodopa and bilateral subthalamic stimulation," *Journal of Neurology, Neurosurgery & Psychiatry,* vol. 68, no. 5, pp. 595-600, 2000.

[132] M. Cassidy *et al.*, "Movement related changes in synchronization in the human basal ganglia," *Brain,* vol. 125, no. 6, pp. 1235-1246, 2002.

[133] R. Jiang, B. H. Jansen, B. R. Sheth, and J. Chen, "Dynamic multi-channel TMS with reconfigurable coil," *IEEE Transactions on Neural Systems and Rehabilitation Engineering,* vol. 21, no. 3, pp. 370-375, 2013.